الجمـــهورية الجزائرية الديمـــقراطية الشعـــبية
DEMOCRATIC AND POPULAR REPUBLIC OF ALGERIA
وزارة التعـلـيـم الـعـالـــي والـبـحـث الـعـلـمي
MINISTERY OF HIGHER EDUCATION AND SCIENTIFIC RESEARCH
جـامـعـــة عمّـــار ثـلـيـــجـــي بالاغـــــــــواط
UNIVERSITY AMAR TELIDJI LAGHOUAT

كـلـيـــــة التكنولوجـــيـــــــا
FACULTY OF TECHNOLOGY
قســـم الالكترونيك
DEPARTEMENT OF ELECTRONICS

Master's Thesis

Domaine : Science and Technology

Sector : Telecommunications

Option : Networks and telecommunications

Presented by:
Benchaoui Fatima Zahraa

THEME

Characterization of Metamaterials for the Fabrication of Printed Antennas

Publicly supported before the jury composed of :

Name	Grade	Quality
Chouireb Fatima	Professor	President
Bensafieddine Djalal	MCA	Examinator
SALEH Chaker	MCA	Co-rapportor
Bouzouad Mouloud	Professor	Supervisor

Année Universitaire 2024/2025

Acknowledgements

I would like to acknowledge and give my warmest thanks to my supervisor Professor Bouzouad Mouloud for his support and my Co-Supervisor Dr Chaker Saleh who made this work possible, his guidance and advice carried me through all the stages of making and writing my project.

My appreciation also goes to the faculty and staff in the Department of Electronic engineering at University Ammar thlidji, whose resources and assistance have been invaluable. I would also like to acknowledge my peers for their camaraderie and the stimulating discussions that inspired me throughout my academic journey. Their collective wisdom and encouragement have been a cornerstone of my research experience.

And finally this thesis is a reflection of the unwavering support and boundless love I received from my family and friends during this challenging academic pursuit. I owe an immense debt of gratitude to my parents, who nurtured my curiosity and supported my educational endeavours from the very beginning.

Dedication

I dedicate this humble work to everyone who helped supporting me and been with me through it all.

My dear parents, my family, my friends and my professors words can never express the gratitude I feel or how thankful to you I am.

This wouldn't have happened without you.

الملخص

تتناول هذه الأطروحة تصميم ومحاكاة وتصنيع خلية فائقة من المواد الخارقة (الميتاماتيريال) قابلة لإعادة التشكيل، مخصصة للتحكم الديناميكي في ترددات تشغيل الهوائيات المطبوعة. تكمن الابتكار الأساسي في خلية فائقة بحجم 4x4تتكون من نوعين من الخلايا الوحدوية بأبعاد 3x3 ملم²: نوع متصل على شكل صليب (A) يُظهر معامل انكسار قريب من الصفر، ونوع منفصل على شكل صليب (B) بمعامل انكسار أكبر قليلاً من الواحد. تتيح آلية تبديل جديدة قابلة لإعادة التشكيل ترتيبًا مكانيًا ونسبة مئوية عشوائية لهذين النوعين من الخلايا الوحدوية، مما يوفر تحكمًا ديناميكيًا في الاستجابة الكهرومغناطيسية للخلية الفائقة. يضمن دورة الخلية الوحدوية (3 ملم) التشغيل تحت الطول الموجي عند 2.4 جيجاهرتز. قامت محاكاة كهرومغناطيسية مفصلة بتوصيف تكوينات مختلفة، مما أظهر القدرة على التحكم في التردد الرنيني لهوائي رقعي مدمج عن طريق تغيير نسبة الخلايا الوحدوية المنفصلة (6.25%، 12.5%، 18.75%، 25%) وتوزيعها المكاني. يؤسس هذا العمل طريقة قوية لضبط التردد في الوقت الفعلي، مما يقدم تطورات كبيرة لأنظمة الهوائيات الذكية التكيفية والمرنة في الاتصالات اللاسلكية الحديثة.

الكلمات المفتاحية: المواد الخارقة, الخلايا الفائقة

Abstract

This thesis presents the design, simulation, and fabrication of a reconfigurable metamaterial supercell intended for dynamic control of printed antenna operating frequencies. The core innovation involves a 4x4 supercell composed of two types of 3x3 mm² unit cells: a connected cross-type (A) exhibiting a near-zero refractive index, and a disconnected cross-type (B) with a refractive index slightly greater than unity. A novel reconfigurable switching mechanism allows for arbitrary spatial arrangement and proportion of these unit cell types, enabling dynamic control over the supercell's electromagnetic response. The unit cell period (3 mm) ensures subwavelength operation at 2.4 GHz. Detailed electromagnetic simulations characterized various configurations, demonstrating the ability to control the resonant frequency of an integrated patch antenna by varying the percentage of disconnected unit cells (6.25%, 12.5%, 18.75%, 25%) and their spatial distribution. This work establishes a robust method for real-time frequency

tuning, offering significant advancements for adaptive and flexible smart antenna systems in modern wireless telecommunications.

Key words : Metamaterials, Supercells

Résumé

Cette thèse présente la conception, la simulation et la fabrication d'une supercellule de métamatériau reconfigurable destinée au contrôle dynamique des fréquences de fonctionnement des antennes imprimées. L'innovation majeure réside dans une supercellule 4x4 composée de deux types de cellules unitaires de 3x3 mm² : un type en croix connectée (A) présentant un indice de réfraction quasi nul, et un type en croix déconnectée (B) avec un indice de réfraction légèrement supérieur à l'unité. Un nouveau mécanisme de commutation reconfigurable permet un arrangement spatial et une proportion arbitraires de ces types de cellules unitaires, offrant un contrôle dynamique de la réponse électromagnétique de la supercellule. La période de la cellule unitaire (3 mm) assure un fonctionnement sublongueur d'onde à 2,4 GHz. Des simulations électromagnétiques détaillées ont caractérisé diverses configurations, démontrant la capacité à contrôler la fréquence de résonance d'une antenne patch intégrée en faisant varier le pourcentage de cellules unitaires déconnectées (6,25 %, 12,5 %, 18,75 %, 25 %) et leur répartition spatiale. Ce travail établit une méthode robuste pour l'accord de fréquence en temps réel, offrant des avancées significatives pour les systèmes d'antennes intelligentes adaptatives et flexibles dans les télécommunications sans fil modernes.

Mots clés : Métamatériaux, Supercellules

Contents

Chapter III: Metamaterial based Antennas

List of Figures

List of Tables

General Introduction

The advancement of wireless telecommunications networks necessitates the development of smart antenna systems. To ensure optimal quality of service, it is essential to steer and antenna operating frequency and control the radiation pattern of antennas in desired directions—a goal increasingly achieved through the integration of smart materials, which enable dynamic reconfiguration, adaptive and enhanced electromagnetic parameters.

Materials can be broadly categorized as conductors or dielectrics based on their constitutive parameters—such as dielectric permittivity, magnetic permeability, and refractive index—which govern their electromagnetic behavior. In recent years, metamaterials, which are artificially engineered structures with unique electromagnetic properties, have attracted significant interest due to their tunable and programmable nature.

This work focuses on the design , simulation and fabrication of metamaterial supercells composed of 4×4 unit cells, each with dimensions of 3 mm × 3 mm. Two types of unit cells are explored: the connected cross type(A) , which exhibits a near-zero refractive index, and the disconnected cross type (B) , characterized by a refractive index slightly greater than unity. A novel aspect of this design is the ability to switch each unit cell between these two types via a reconfigurable switching mechanism, enabling dynamic control over the electromagnetic response of different regions of the supercell. This programmable structure allows for the creation of arbitrary refractive index patterns across the metamaterial supercell.

To ensure subwavelength operation and satisfy the homogenization criterion, the unit cell period was set to 3 mm, significantly smaller than the free-space wavelength of 125 mm at the operating frequency of 2.4 GHz. Various configurations were simulated by adjusting the proportion and spatial distribution of type B (disconnected) unit cells within the supercell, with the aim of analyzing the resulting electromagnetic behavior and identifying the most effective design.

General introduction

The final goal of this research is to integrate the reconfigurable metamaterial supercell into the design of a smart antenna. By dynamically modifying the connectivity of the unit cells, the antenna can adapt its operating frequency and radiation characteristics in real time, enabling enhanced performance and flexibility in modern communication systems.

This thesis is organized into three main chapters:

Chapter one deals with the definition of metamaterials and their applications. The second chapter is devoted to the effective parameters extraction of homogenized metamaterials supercell [1] .

Finally, Chapter 3 focuses on controlling the antenna's operating frequency through the design of metamaterial supercells, each consisting of 16 unit cells. These supercells are composed of two types of metamaterial elements: connected cross-type A and disconnected coss-type B. Frequency tuning is achieved by varying both the number and arrangement of disconnected cross-type B elements within the supercell.

Four configurations are studied, corresponding to different percentages of disconnected unit cells:

6.25%: one disconnected cross-type B and fifteen connected (A)

12.5%: two disconnected and fourteen connected

18.75%: three disconnected and thirteen connected

25%: four disconnected and twelve connected

The disconnected elements can be positioned arbitrarily within the supercell to form different spatial patterns. By manipulating the switching states of the unit cells, the electromagnetic characteristics of the supercell can be dynamically reconfigured. This enables effective control of the patch antenna's resonant frequency.

Chapter I

General overview of Smart Materials

I- General overview of Smart Materials

I.1 Introduction

In recent years, the field of materials science has witnessed groundbreaking advancements with the emergence of smart materials. These innovative materials possess unique properties that enable them to respond to environmental stimuli, making them highly adaptable and versatile.

The concept of smart materials is rooted in their ability to integrate sensing, actuation, and control at the material level, thereby enabling autonomous behavior.

In parallel with the evolution of smart materials, a groundbreaking paradigm in materials science has emerged with the advent of metamaterials. These extraordinary engineered materials derive their properties from their meticulously designed, sub-wavelength artificial structures. By manipulating the geometry, size, and arrangement of these constituent elements.. While distinct in their primary design philosophy—smart materials often focus on intrinsic responsive properties, while metamaterials emphasize structural design for exotic wave manipulation—the lines between these two fields are increasingly blurring. The integration of responsive elements into metamaterial designs creates "smart metamaterials" allowing their unique properties to be dynamically tuned or switched in response to external stimuli. This fusion promises an even more profound impact, offering unprecedented control over energy, information, and physical interactions.

This chapter aims to provide a comprehensive general overview of smart materials, laying the groundwork for understanding their significance and potential. Furthermore, it will introduce the fascinating realm of metamaterials, exploring their distinctive characteristics and highlighting the synergistic opportunities that arise from their combination with smart material principles. Together, smart materials and metamaterials

represent a frontier of materials science, paving the way for revolutionary technologies that can actively interact with and reshape our world.

I.2 Smart Materials

The concept of smart materials dates back to the early 20th century, with the term "smart material" gaining popularity in the 1980s. Early examples include piezoelectric materials and shape memory alloys, which have been used for decades in sensors and actuators, the development of advanced polymers and nanomaterials has accelerated the field in recent years. Smart materials are a family of materials that are listed in advanced materials. [2]

These materials are considered “smart” because they can autonomously change their properties, such as physical (pressure, temperature, humidity, light, electric field, magnetic field), chemical (pH, CO2, etc.), or biological stimuli . Unlike conventional materials with static properties, smart materials possess a responsiveness that isn’t just a passive reaction, but an engineered intelligence that enables them to perform specific functions such as adapt, self-heal, or change their characteristics—such as shape, color, stiffness, or electrical conductivity without any human intervention. [3]

Smart materials are engineered to respond to their environment and switch back to their original state once the stimulus is removed. They operate by integrating sensing and actuation mechanisms at the molecular or structural level. For example, piezoelectric materials convert mechanical energy to electrical energy, while shape memory alloys undergo phase changes that allow them to "remember" and return to a specific shape. [2] [3] [4]

Smart materials are making their mark across a wide range of industries, from self-repairing concrete in construction to color-changing camouflage developed for the defense sector. One of the most common types, shape-memory alloys, return to their original shape under heat, making them ideal for applications in medical devices, robotics

and actuators. Meanwhile, piezoelectric materials are being installed into sensors, speakers and energy-harvesting systems for their unique ability to convert mechanical energy into electrical energy. [5]

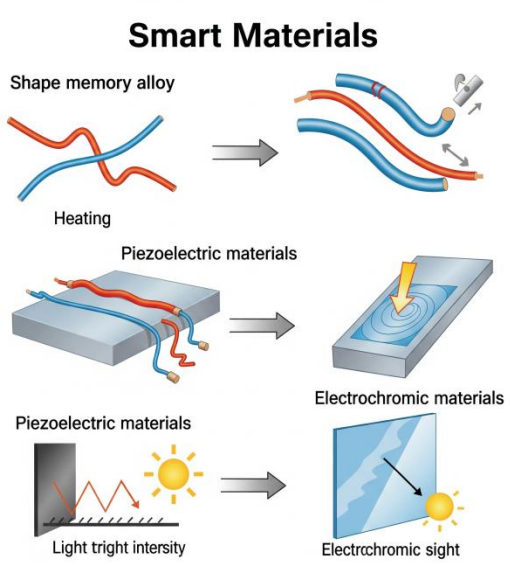

Figure I.1 Smart materials

I.2.1 Types of smart materials

There are a number of types of smart material, of which are already common. Some examples are as following:

- Piezoelectric materials are materials that produce a voltage when stress is applied. Since this effect also applies in a reverse manner, a voltage across the sample will produce stress within sample. Suitably designed structures made from these materials can, therefore, be made that bend, expand or contract when a voltage is applied.
- Shape-memory alloys and shape-memory polymers are materials in which large deformation can be induced and recovered through temperature changes or stress changes (pseudoelasticity). The shape memory effect results due to respectively martensitic phase change and induced elasticity at higher temperatures. A common example is Nitmol.
- Photovoltaic materials or optoelectronics convert light to electrical current.

- Electroactive polymers (EAPs) change their volume by voltage or electric fields.
- Magnetostrictive materials exhibit a change in shape under the influence of magnetic field and also exhibit a change in their magnetization under the influence of mechanical stress.
- Magnetic shape memory alloys are materials that change their shape in response to a significant change in the magnetic field.
- Smart inorganic polymers showing tunable and responsive properties.
- pH-sensitive polymers are materials that change in volume when the pH of the surrounding medium changes.
- Temperature-responsive polymers are materials which undergo changes upon temperature.
- Halochromic materials are commonly used materials that change their color as a result of changing acidity. One suggested application is for paints that can change color to indicate corrosion in the metal underneath them.
- Chromogenic systems change color in response to electrical, optical or thermal changes. These include electrochromic materials, which change their colour or opacity on the application of a voltage (e.g., liquid crystal displays), thermochromic materials change in colour depending on their temperature, and photochromic materials, which change colour in response to light—for example, light-sensitive sunglasses that darken when exposed to bright sunlight.
- Ferrofluids are magnetic fluids (affected by magnets and magnetic fields).
- Photomechanical materials change shape under exposure to light.
- Polycaprolactone (polymorph) can be molded by immersion in hot water.
- Self-healing materials have the intrinsic ability to repair damage due to normal usage, thus expanding the material's lifetime.
- Dielectric elastomers (DEs) are smart material systems which produce large strains (up to 500%) under the influence of an external electric field.

- Magnetocaloric materials are compounds that undergo a reversible change in temperature upon exposure to a changing magnetic field.
- Thermoelectric materials are used to build devices that convert temperature differences into electricity and vice versa.
- Chemoresponsive materials change size or volume under the influence of external chemical or biological compound. [6]

I.3 Metamaterials

Metamaterials are engineered composite materials that exhibit unique properties not found in naturally occurring materials. These properties arise from their designed internal micro- or nano-structures rather than their chemical composition alone. Metamaterials have revolutionized materials science by enabling novel electromagnetic, acoustic, and mechanical wave manipulations. Their ability to control wave propagation has led to breakthroughs in invisibility cloaks, superlenses, and highly efficient antennas.

Metamaterials consist of periodically or randomly distributed artificial structures that have a size and spacing much smaller than the wavelengths of incoming electromagnetic radiation. Consequently, the microscopic details of these individual structures cannot be resolved by the wave. For example, it is difficult to view the fine features of metamaterials that operate at optical wavelengths with visible light, and shorter-wavelength electromagnetic radiation, such as an X-ray, is needed to image and scan them. Researchers can approximate the assemblage of inhomogeneous individual structures as a continuous substance and define their effective material properties at the macroscopic level. Essentially, each artificial structure functions as an atom or a molecule functions in normal materials. However, when subjected to regulated interactions with electromagnetic radiation, the structures give rise to entirely extraordinary properties. (Some naturally occurring materials such as opal and vanadium oxide do exhibit unusual properties when they interact with electromagnetic radiation and

have been called “natural metamaterials.” However, metamaterials are most often known as artificially occurring materials). [7] [8]

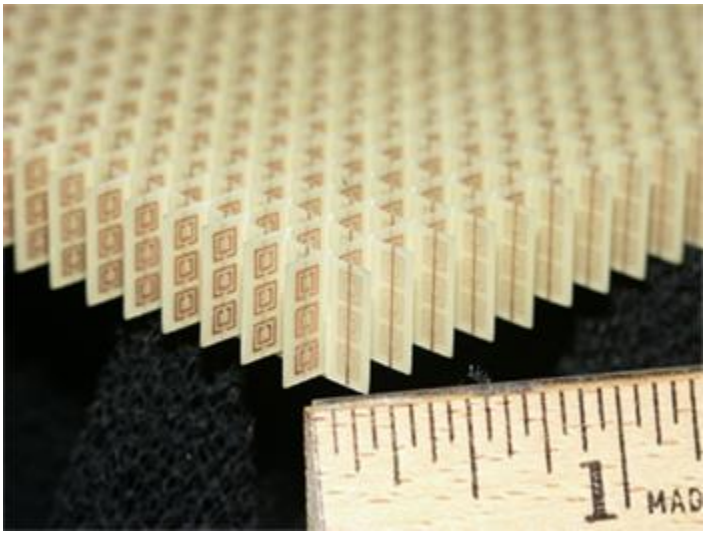

Figure I.2 Metamaterials

I.3.1 Key Characteristics and Principles

Structural Basis: Metamaterials derive their properties from their shape, geometry, size, orientation, and arrangement of their constituent elements rather than the materials themselves.

Wave Manipulation: They can affect waves of electromagnetic radiation or sound in ways not observed in bulk materials, including exhibiting a negative index of refraction.

Negative-Index Metamaterials: These are a special class that can refract light negatively, enabling novel optical effects like superlensing.

I.3.2 Metamaterials Analytical Models

To understand the frequency-dependent electromagnetic behavior of materials, including the engineered responses of metamaterials, classical models are essential. The Drude and Lorentz models describe how charge carriers interact with electromagnetic waves, yielding insights into a material's complex permittivity $\epsilon(\omega)$.

The Drude Model: Free Electron Response

The Drude model describes the electrical conductivity and optical properties of metals (and plasmas) by treating conduction electrons as a gas of free, colliding particles. When

an oscillating electric field is applied, these electrons accelerate, leading to a current, with collisions acting as a damping force. [9]

The complex frequency-dependent permittivity ϵ(ω) derived from the Drude model is given by:

$$\epsilon(\omega) = \epsilon_0(1 - \frac{\omega_p^2}{\omega^2 + i\gamma}) \qquad (I.1)$$

where:

ϵ_0: Permittivity of free space.

ω: Angular frequency of the incident wave.

$\omega_p = \sqrt{\frac{ne^2}{m_e \epsilon_0}}$: Plasma frequency, representing the collective oscillation of free electrons (n: electron density, e: elementary charge, m_e: electron mass).

γ: Damping rate (collision frequency) of electrons.

Physically, for ω≪ωp, metals exhibit a large negative real part of ϵ(ω), explaining their high reflectivity. This negative permittivity is a key characteristic exploited in many metallic components of electromagnetic metamaterials (e.g., metallic wires in epsilon-negative (ENG) or left-handed materials (LHMs)). [10] [11]

The Lorentz Model: Bound Electron Resonances

The Lorentz model describes the dielectric response of materials with bound electrons (insulators, semiconductors, or resonant elements). It models electrons as being harmonically bound to atomic nuclei by a spring-like force, driven by an external oscillating electric field and subject to damping. This induced oscillation creates microscopic electric dipoles, contributing to the material's polarization. [12]

For a single resonance, the complex frequency-dependent permittivity ϵ(ω) is expressed as:

$$\epsilon(\omega) = \epsilon_0(1 + \frac{F\omega_p^2}{\omega_p^2 - \omega^2 + i\gamma\omega}) \qquad (I.2)$$

where:

F: Oscillator strength, related to the density of bound electrons.

ω_p: Plasma frequency, scaling the strength of the resonance.

ω_0: Resonant frequency of the bound electrons.

γ: Damping rate for the bound oscillations.

The Lorentz model predicts strong dispersion around ω_0, where the material's response changes rapidly, and absorption peaks. This resonant behavior is fundamental to understanding the frequency-selective response of engineered "meta-atoms" in metamaterials (e.g., split-ring resonators), enabling properties like negative permeability at specific frequencies. [11] [12]

The Drude-Lorentz Model: A Combined Approach

For materials or metamaterials exhibiting both free-electron-like conduction and bound-electron (or structural) resonances, a combined Drude-Lorentz model is used. This model superimposes the Drude term and one or more Lorentz terms to provide a comprehensive description of the complex permittivity over a broad frequency range.

The generalized complex permittivity is given by:

$$\epsilon(\omega)= \epsilon_\infty - \frac{\omega_p^2}{\omega^2+i\gamma_D\omega} + \sum_j \frac{F_j\omega_{p,j}^2}{\left(\omega_{0,j}^2-\omega^2\right)+i\gamma_j\omega} \qquad (I.3)$$

where:

ϵ_∞: High-frequency permittivity constant.

The second term is the Drude contribution, with γ_D as its damping rate.

The summation represents multiple Lorentz resonances, each with its specific parameters (F_j,ω_p,j,ω_0,j,γ_j).

This combined model is a powerful analytical tool for designing and characterizing metamaterials. By accurately modeling the interplay between conductive elements (Drude-like) and resonant meta-atoms (Lorentz-like), it allows for precise engineering of the material's effective electromagnetic parameters ($\epsilon_{\text{eff}}(\omega)$ and $\mu_{\text{eff}}(\omega)$), leading to the realization of unconventional properties such as negative refractive index. [13]

I.4 Classification

Metamaterials are classified into several distinct classes, based upon modified properties of the materials they are thermal, acoustic/transport, electromagnetic and mechanical.

I.4.1 Acoustic Metamaterials

Acoustic Metamaterials are developed by combining two or more than two materials with distinct density and bulk modulus. They can have negative density, negative emastic modulus and anisotropic mass. These metamaterials can be further divided into three distinct categories: Phonic crystals, resonant structure and space coiling.

Phonic crystals generally contain resonating sites as well as regular arrays of acoustic scattering within the material and provide periodicity in their structure. The Resonant structures are the type of metamaterial that are utilized for sound control and acoustic filtering. The Space coiling metamaterial provide Fabry-Perot resonances and are used in conditions where the waves can be guided without cut-off.

I.4.2 Electromagnetic metamaterials

Electromagnetic metamaterials are a type of metamaterial developed by arranging homogeneous metal structures. They are used to sense humidity, pressure, biological molecules that are present in the environments and are characterized based on the following features:

Refractive Index

The refractive index *n* of metamaterials can be negative over certain frequency ranges, leading to so-called negative-index metamaterials (NIMs) or left-handed materials. This means that electromagnetic waves refract oppositely compared to conventional materials, enabling unusual phenomena such as reversed Snell's law and backward wave propagation. [15]

The negative refractive index arises from the simultaneous negativity of both effective permittivity and permeability in the metamaterial, which is achieved by designing the geometry of the unit cells rather than relying on the intrinsic properties of the constituent materials. [15] [16]

Permittivity (ε) and Permeability (μ)

Effective permittivity (ε) and effective permeability (μ) are frequency-dependent and can be engineered to be negative in metamaterials. For example, arrays of metallic wires can produce negative permittivity in certain frequency bands, while split-ring resonators (SRRs) can produce negative permeability. [16]

When both ε and μ are negative simultaneously, the metamaterial exhibits a negative refractive index. [16]

These effective parameters are not simply those of the base materials but are emergent properties resulting from the structure's periodic arrangement and geometry at scales smaller than the wavelength of the incident electromagnetic wave. [15] [16]

I.4.3 Mechanical Metamaterials

Mechanical metamaterials consist of negative elastic modulus, zero Shear modulus, and negative Poisson's ratio. Materials with negative Poisson's ratio have property to stiffer when the value of load increases. Also, they provide good sound and vibration absorption due to which they're used extensively in defense and aerospace applications. [14]

I.5 Supercells

Metamaterial supercells are advanced building blocks used in the design of metasurfaces and metamaterials, enabling functionalities beyond what is possible with simple, repeating unit cells. Unlike conventional metasurfaces composed of identical subwavelength elements (meta-atoms), supercells are larger structures formed by grouping multiple meta-atoms together. This configuration allows the exploitation of both the individual properties of each meta-atom and the interactions (coupling) between them, resulting in novel optical responses and enhanced control over wave manipulation

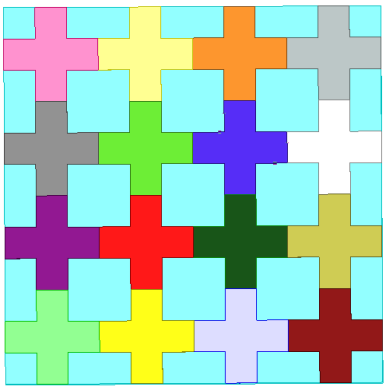

Figure I.3 A design of a supercell

Non-local Effects: By merging adjacent unit cells into a supercell, designers can account for non-local optical effects-interactions between neighboring meta-atoms-which are critical for achieving complex functionalities such as large-angle beam steering and multifunctional responses

Diffraction Orders: When supercells are periodically arranged, the resulting device behaves like a metagrating, splitting light into multiple diffraction orders. The size and arrangement of the supercell determine the number and direction of these orders

Independent Control: Each supercell can be optimized to provide specific phase and amplitude responses for each diffraction order, enabling independent and simultaneous manipulation of multiple optical functions (e.g., focusing, holography, polarization control). [17]

I.6 Applications

Metamaterials are used as antennas in the medical sector to increase the radiated power as well as matching the characteristics and efficiency bandwidth performance of an antenna system. Also, it minimizes the mutual coupling between the antenna parts. They’re used in automotive sector to operate the motors using electricity and to ensure electromagnetic compatibility. Now-a-days, bio sensing method based on metamaterials are preferred due to their less cost and label-free biomolecule detection. Based on the frequency of sensing biomolecule the sensors are characterized as plasmatic biosensor, microwave biosensor,

and terahertz biosensor. In addition, metamaterials find application in MEMS, spectroscopy, light and sound filtering, etc. [14]

Superlenses and Imaging: Negative-index metamaterials allow imaging beyond the diffraction limit, enabling super-resolution microscopes and high-precision lithography.

Invisibility Cloaks: By bending light around an object, metamaterials can render objects effectively invisible at certain frequencies, promising stealth technology innovations.

Antennas and Waveguides: Metamaterial antennas improve radiated power, reduce size, increase directivity, allow tunable frequencies and making Compact, highly efficient antennas with beam-steering and frequency agility are designed utilizing electromagnetic metamaterials, advancing wireless communication.

Sensors: Metamaterial-based sensors enhance sensitivity for biochemical detection and environmental monitoring due to strong field localization effects.

Shock Absorption and Vibration Isolation: Metamaterial absorbers can absorb large amounts of electromagnetic radiation, They also absorb impacts and isolate vibrations in automotive and aerospace components. useful in photodetection and solar photovoltaics.

Acoustic Cloaking and Noise Control: Acoustic metamaterials manage sound wave propagation to create zones of silence or redirect noise, useful in architectural acoustics and ultrasonic devices.

Programmable Materials: Mechanical metamaterials with embedded smart materials can change shape or stiffness on-demand, leading to soft robotics, adaptive prosthetics, and deployable structures.

Radar Cross-Section Reduction: Used in stealth technology to reduce radar detectability by absorption or redirecting scattered energy.

Seismic Protection: Designed to counteract seismic waves, protecting buildings and infrastructure.

Sound Filtering: Nanostructured metamaterials can control sound waves for applications like medical diagnostics and sound suppression.

Guided Mode Manipulations: Integrated with optical waveguides to control light propagation at nanoscale, enabling devices like polarization beam splitters and on-chip biosensors.

Energy Transfer and Sensors: Metamaterial-based metadevices include near-field energy transfer devices, metamaterial mirrors, biosensors, and quantum-cascade detectors.

Soft Robotics and Real-Time Adaptability: Recent advances include metamaterials that can dynamically tune their shape and mechanical properties in real time, inspired by biological adaptability, opening new

Recent advances in additive manufacturing have accelerated these applications by allowing the fabrication of intricate mechanical metamaterial geometries with embedded active materials. [18]

I.7 Conclusion

This chapter has provided a foundational overview of smart materials, highlighting their unique ability to sense and respond dynamically to external stimuli. Their inherent adaptive functionalities, from shape memory to piezoelectricity, mark a significant advancement beyond passive materials, enabling autonomous behaviors critical for modern technologies.

Concurrently, we introduced metamaterials, emphasizing that their extraordinary properties stem from meticulously engineered sub-wavelength structures rather than chemical composition. These materials offer unprecedented control over wave phenomena.

The convergence of these two fields, leading to reconfigurable metamaterials, represents a powerful synergy. Both smart materials and metamaterials are at the forefront of materials science, driving innovation by offering dynamic, responsive, and intelligently designed functionalities. Their continued development promises to revolutionize diverse fields, from intelligent sensing to advanced robotics, laying the groundwork for future technological breakthroughs.

Chapter II

Characterization of Supercells

II- Characterization of Supercells

II.1 Introduction

We can categorize a material as either a conductor or a dielectric based on its constitutive parameters, such as dielectric permittivity, magnetic permeability, and refractive index, which define its electromagnetic behavior. In this chapter (Simulation part) we are designing metamaterial supercells (4X4) which is composed of 16 unite cells where a=3mm (a is the length and width of the unit cell) This metamaterial supercells was based on a connected and a disconnected cross type unit cell. The behaviors and the structure of these connected and disconnected cross type metamaterials have drawn our attention. In one hand, the connected cross type metamaterial behaves like a medium with a close to zero refractive index, while the disconnected cross type metamaterial behaves like a refraction index slightly above unity. In another hand, we noticed an interesting thing, the connected and disconnected unit cells can be gathered in a single one by using an adequate switching system. Depending on the switches states (ON or OFF) we can make the unit cell flipping from the connected the disconnected cross type, This agile unit cell (pixel), allows us to program the behavior of any regions of arbitrary shapes and sizes in the metamaterial supercells as a medium with a refraction index slightly close to unity or as medium with a close to zero refraction index, as depicted in **Figure II.3**.

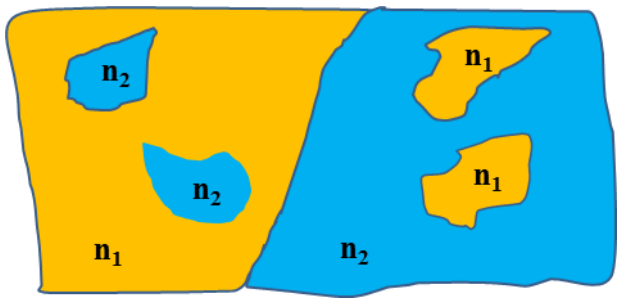

Figure II.1 Agile surface with different regions to different form and with two refraction indices n_1 and n_2

The unit cell sizing begins with the determination of the metamaterial period a. This dimension is directly related to the wave frequency and, therefore, to the homogenization criterion. A metamaterial can be perceived as a homogeneous medium by electromagnetic waves propagating through it, provided that the structural period a is much smaller than the wavelength ($a \ll \lambda$).

In this work, the antenna operates at a frequency of 2.4 GHz, which corresponds to a free-space wavelength of approximately 125 mm. To satisfy the homogenization criterion, the period a must be much smaller than $\lambda/3 \approx 41.7$ mm. Accordingly, we select a = 3 mm ($a \ll \lambda$), to maximize the number of unit cells in the metamaterial grid and ensure subwavelength operation. We chose to design 4 different cases changing α (the percentage of unite cells type B (disconnected) in the supercell) and multiple patterns by changing the position of unite cells type B so that we can study their behavior (conductor or dielectric) and to see which cases and patterns obtain the best results.

finally, we use this supercell-based metamaterial surface to design a smart antenna. The supercells consist of disconnected cross elements in the OFF state, which can be dynamically reconfigured into arbitrary connected geometries (ON state). This reconfigurability enables adaptive control over the antenna's operating frequency and gain, providing high flexibility and enhanced performance in electromagnetic applications. [20]

II.2 Unit cells

II.2.1 Connected unit cell

The ON state of switches constitutes a connected-cross type metamaterial unit cell, as depicted in **Figure II.2**, which is referred to as (type A) in this dissertation. This metamaterial unit cell follows the Drude frequency-dependent model for real part of effective dielectric permittivity.

It presents a one value at the plasma frequency f_p = 21 GHz. The real part of the effective permeability is mostly constant and always close to 0 as shown in **Figure II.3**. the refraction index presents a very inferior real part from 0GHz - 30GHz then starts approaching to 0 after 30GHz.

The imaginary part in all cases represents the loss of the magnetic and electric field.

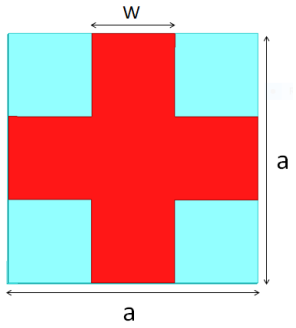

Figure II.2 Unit Cell type A (Connected)

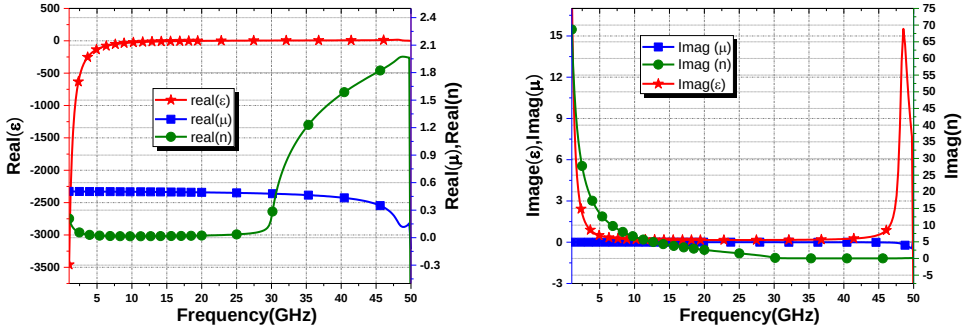

Figure II.3 Type A cell's results (index n, permittivity Ɛ and permeability μ)

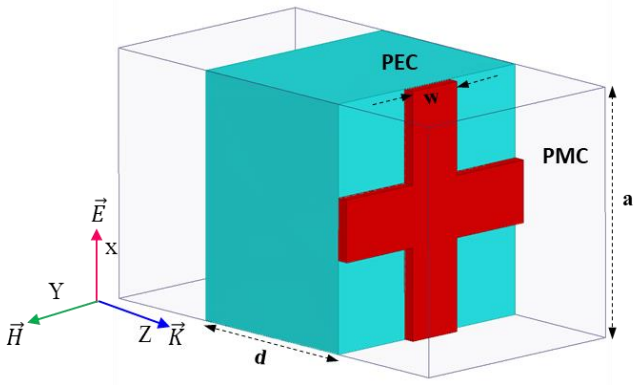

Figure II.4 Boundary conditions of the metamaterial unit cell

To describe the behavior of the supercell metamaterial, the unit cell *S* parameters are retrieved using a commercial code based on the finite element method. The imposed conditions on the unit cell are: i) perfect electric conductor (PEC) in (*xz)* plane which means that the electric field $\vec{E}$ is in the *y* direction and ii) perfect magnetic conductor (PMC) in (*yz*) plane, then, the magnetic field $\vec{H}$ is in the *x* direction The wave propagation is in the *z* direction (wave vector $\vec{k}$ axis) The cross unit cell is simulated over the $20 - 50$ GHz frequency band where the operating frequency f_o = 40 GHz. By assuming that the medium is reciprocal and that the harmonic time dependence is e^{-jwt}.

II.2.2 Disconnected Unit Cell

The OFF state of switches constitutes a metamaterial unit cell type disconnected-cross, as depicted in **Figure II.5** which referred to as (type B) in this dissertation. Dielectric permittivity of this type of metamaterial follows the Lorentz resonant frequency-dependent model. It exhibits a constant value of 6,9 in the real part of effective dielectric permittivity over the frequency range of 0GHz-25GHz then it starts to have peaks at 27GHz, 36GHz and 45GHz, the real effective permeability is close to 1 then has a peak at 27GHz then it goes down close to 0. The real part of the refraction index is constant at 2. as shown in **Figure II.6**.

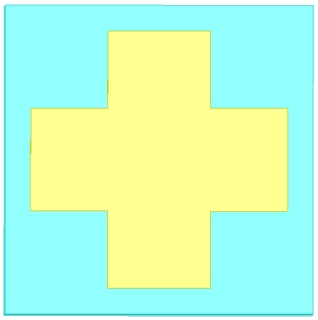

Figure II.5 Unite Cell type B (Disconnected)

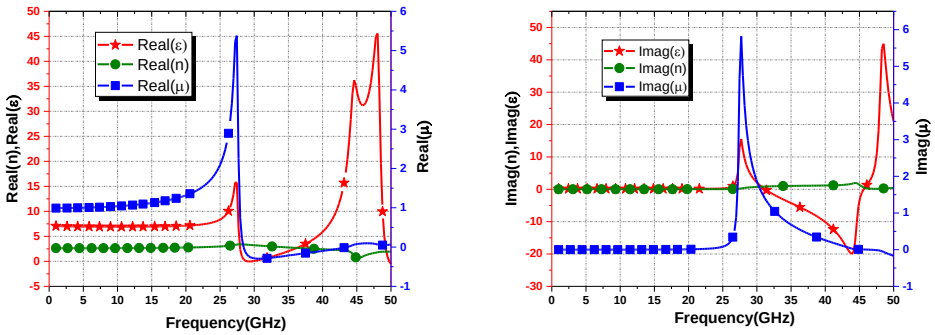

Figure II.6 Type B cell's results (index n, permittivity Ɛ and permeability μ)

II.3 Supercells

II.3.1 Connected Supercell

Figure II.7 represents a design of a supercell with 16 connected unit cells (type A). As we can notice in **Figure II.8** a constant value of 0.47 in the real part of effective permeability over all of the frequency range, a plasma frequency $f_p = 21\text{GHz}$ in real effective permittivity and the real part of the refraction index is almost 0 from 0GHz-30GHz then is peaks at f=49GHZ which are almost the same results (behavior) obtained in the connected unit cell (type A) .

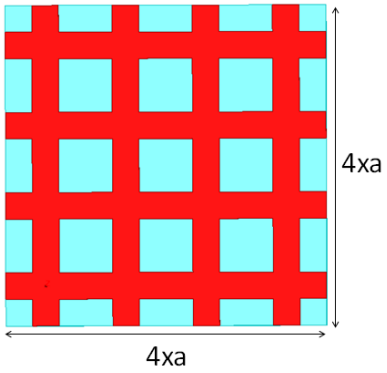

Figure II.7 Connected Supercell

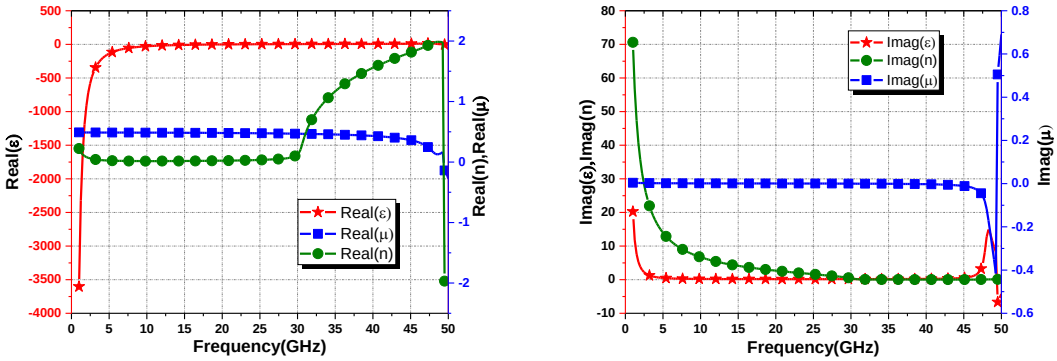

Figure II.8 Results of a Connected Supercell

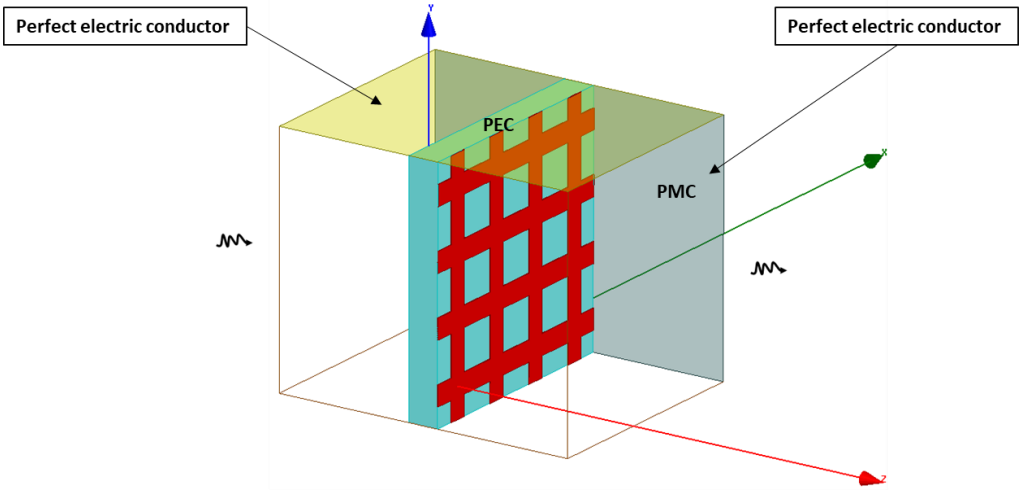

FigureII.9 Boundary conditions of a metamaterial supercell

II.3.2 Disconnected Supercell

Figure II.10 represents a design of a supercell with 16 disconnected unit cells (type B). As we can notice in **Figure II.11** a constant value of 6,6 in the real part of effective permittivity over the frequency range of 0GHz-25GHz then it starts to have peaks at 28GHz and 47.5GHz, the real effective permeability is 1 then has a peak at 28GHz then it goes down close to 0 with negative values. The real part of the refraction index is constant at 2.which are almost the same results (behavior) obtained in the disconnected unit cell (type B) .

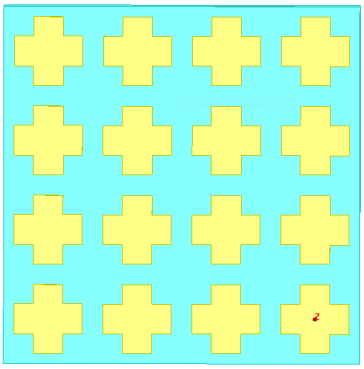

Figure II.10 Disconnected Supercell

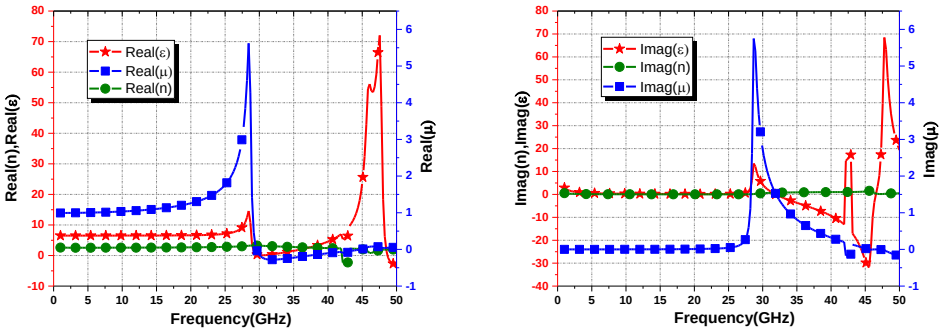

Figure II.11 Results of a Disconnected Supercell

II.4 Cases and Patterns

II.4.1 Case I (α=6.25%)

- Pattern 1

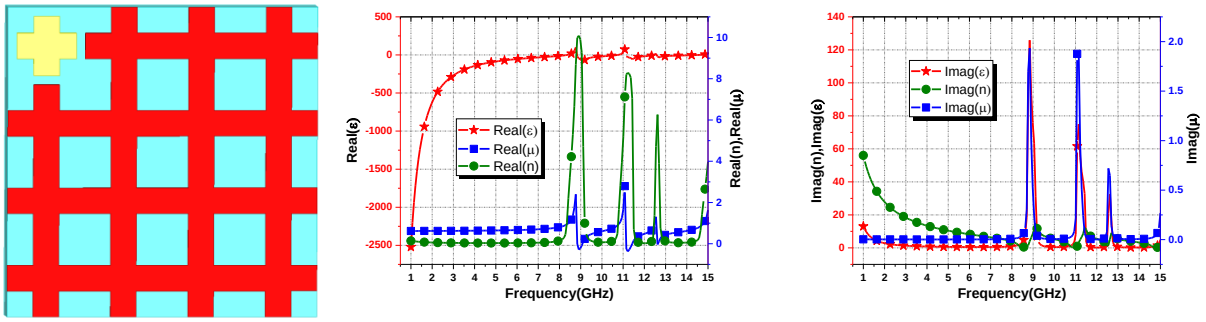

Figure II.12 Pattern1 with one disconnected cell(type B) and 15(type A) cells

- Pattern 2

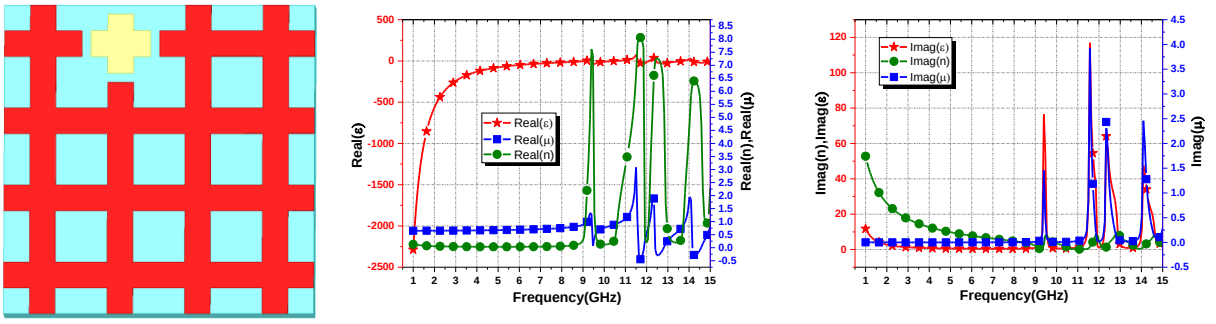

Figure II.13 Pattern2 with one disconnected cell(type B) and 15(type A) cells

- Pattern 3

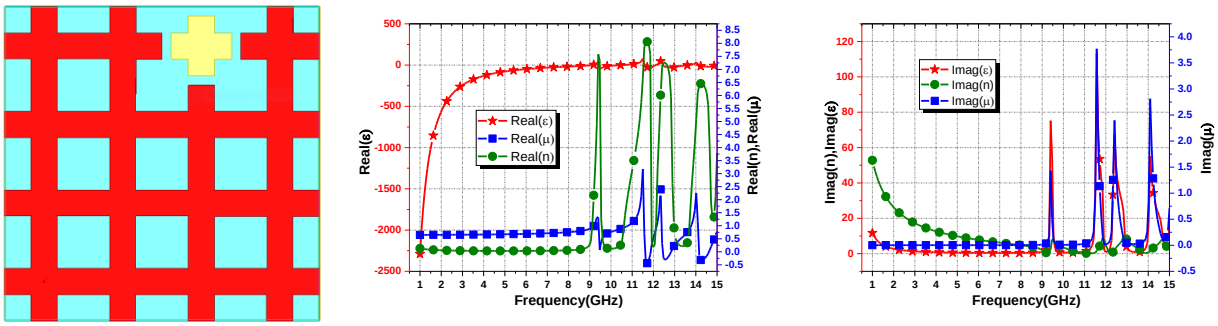

Figure II.14 Pattern3 with one disconnected cell(type B) and 15(type A) cells

- Pattern 4

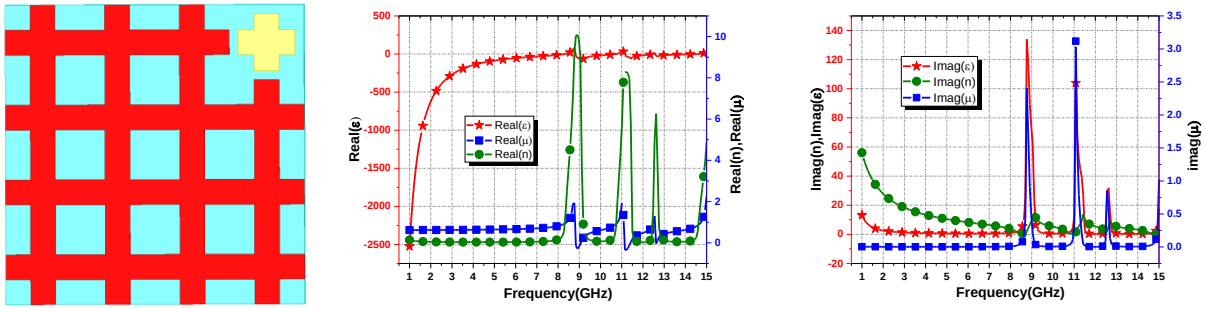

Figure II.15 Pattern4 with one disconnected cell(type B) and 15(type A) cells

- Pattern 5

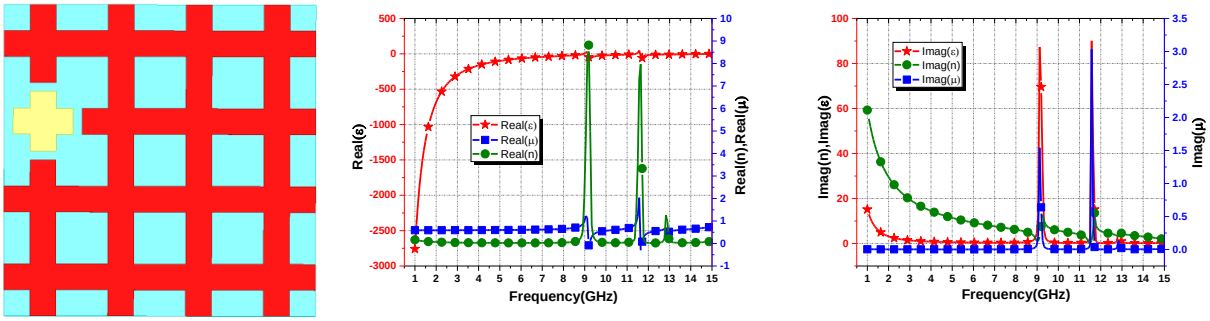

Figure II.16 Pattern5 with one disconnected cell(type B) and 15(type A) cells

- Pattern 6

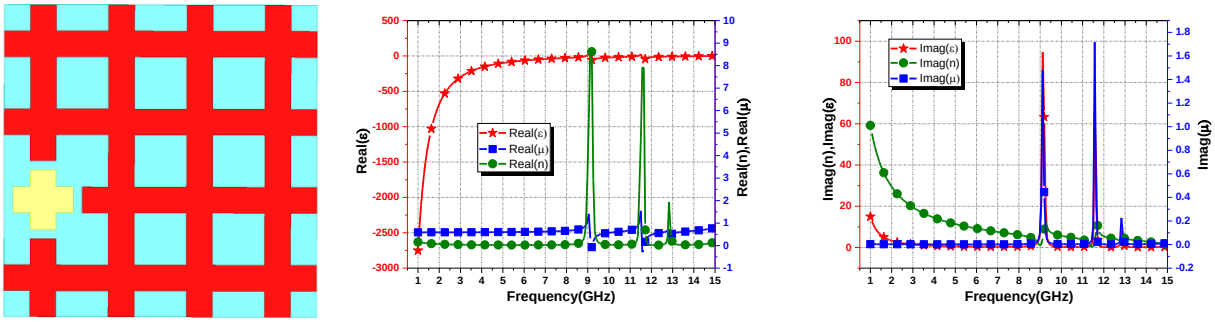

Figure II.17 Pattern6 with one disconnected cell(type B) and 15(type A) cells

- Pattern 7

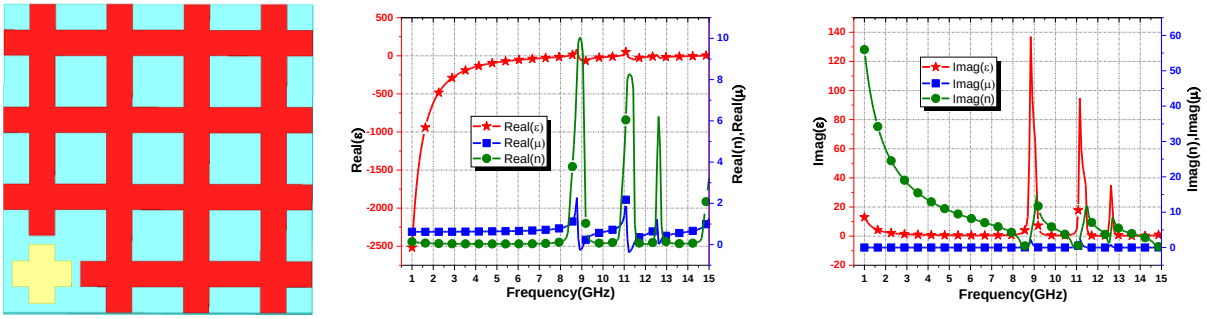

Figure II.18 Pattern7 with one disconnected cell(type B) and 15(type A) cells

- Pattern 8

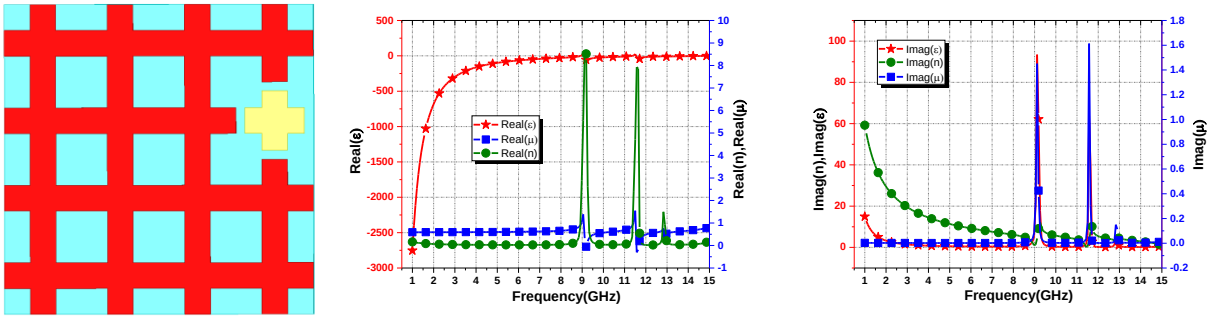

Figure II.19 Pattern8 with one disconnected cell(type B) and 15(type A) cells

- Pattern 9

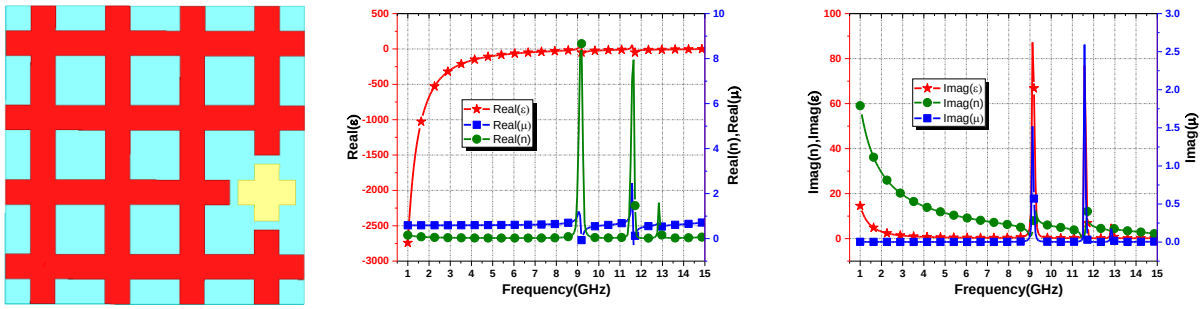

Figure II.20 Pattern9 with one disconnected cell(type B) and 15(type A) cells

- Pattern 10

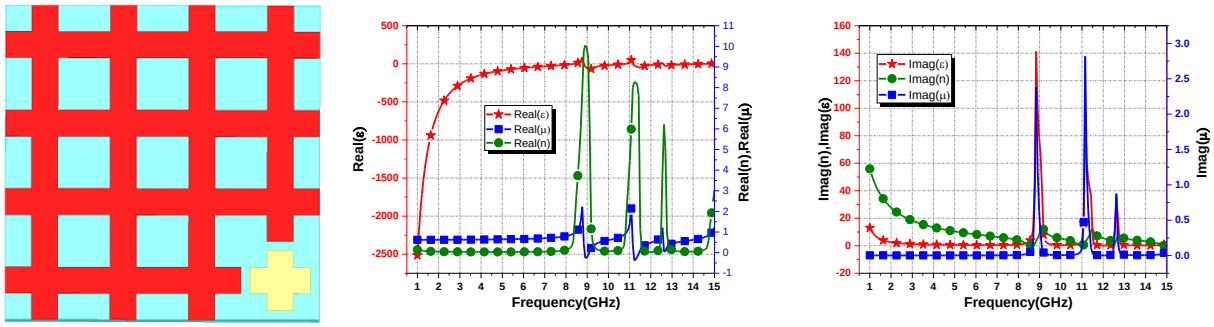

Figure II.21 Pattern10 with one disconnected cell(type B) and 15(type A) cells

In this case (Case I (α=6.25%)) where α is the percentage of disconnected cells (type B)) we have one disconnected cell and 15 connected cells. In each pattern we changed the

position of the disconnected cell. We chose 10 different positions and looking at the results we can see that they are almost identical with very minor differences with a plasma frequency $f_p \approx 8\,\text{GHz}$ in all the patterns, a constant real effective permeability $\mu_{eff} \approx 0$ from 0GHz-9GHz then it starts changing beyond and the same goes to the refractive index with very similar values. We can also notice that the comportment is conductor.

II.4.2 Case II (α=12.5%)

- Pattern 1

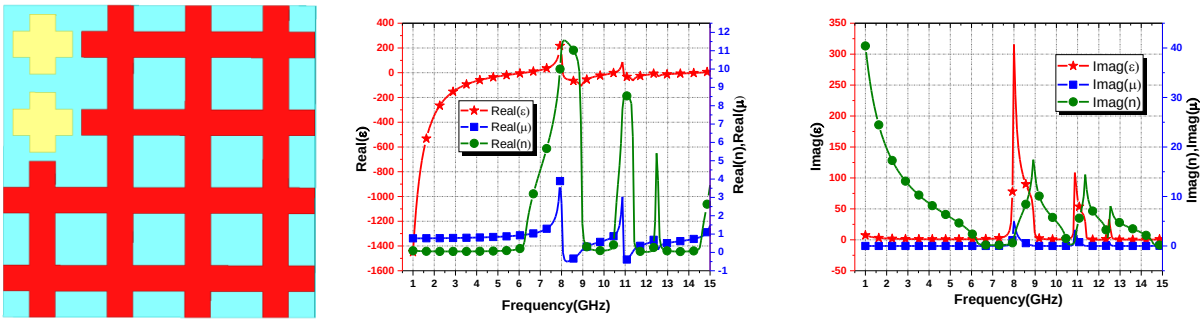

Figure II.22 Pattern1 with 2 disconnected cells(type B) and 14(type A) cells

- Pattern 2

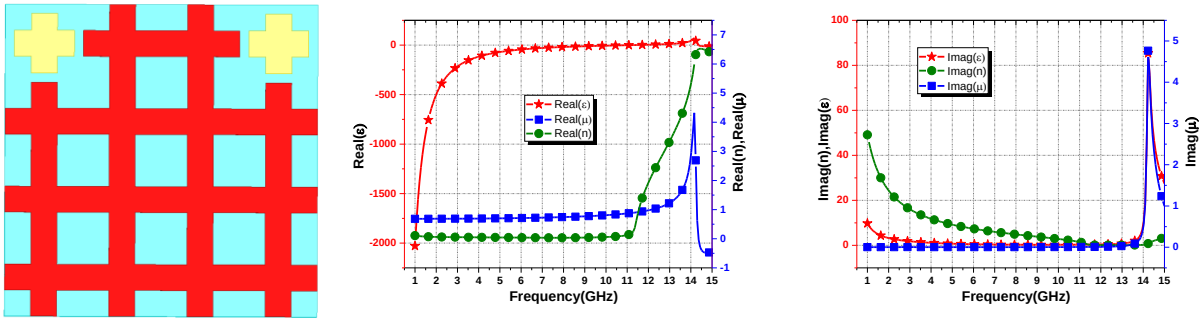

Figure II.23 Pattern2 with 2 disconnected cells(type B) and 14(type A) cells

- Pattern 3

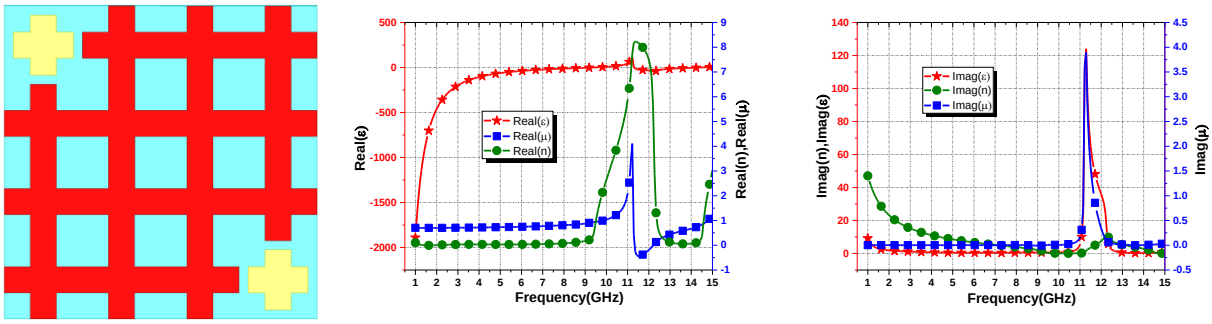

Figure II.24 Pattern3 with 2 disconnected cells(type B) and 14(type A) cells

- Pattern 4

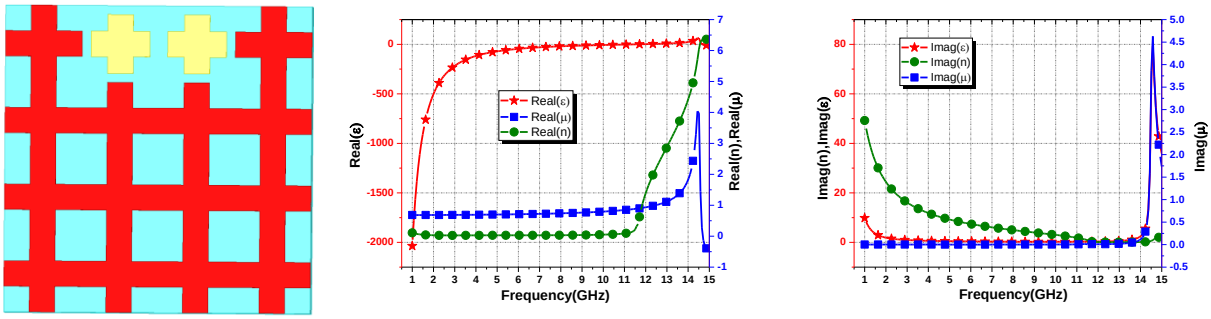

Figure II.25 Pattern4 with 2 disconnected cells(type B) and 14(type A) cells

II.4.3 Case III (α=18.75%)

- Pattern 1

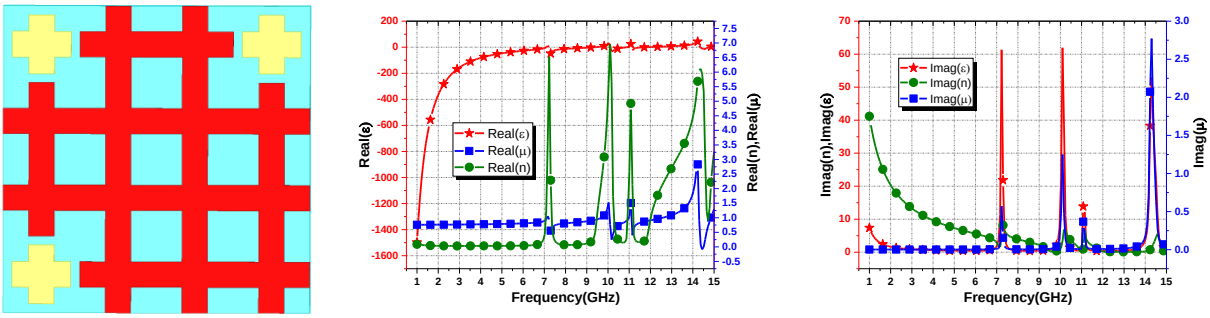

Figure II.26 Pattern1 with 3 disconnected cells(type B) and 13(type A) cells

- Pattern 2

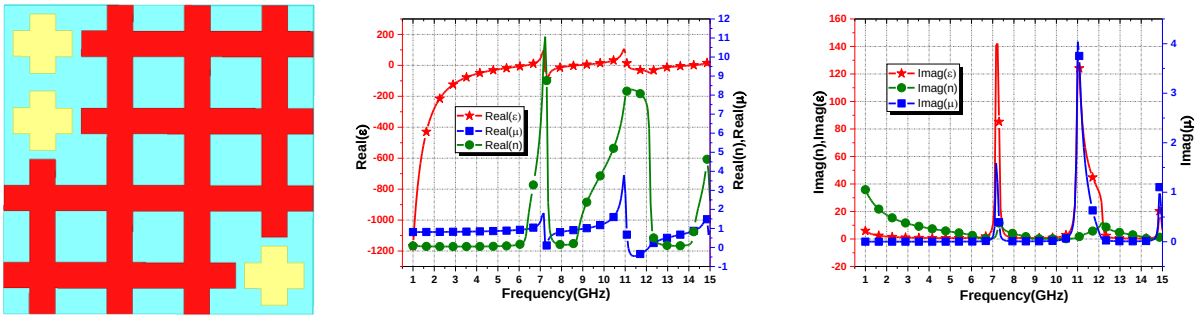

Figure II.27 Pattern2 with 3 disconnected cells(type B) and 13(type A) cells

- Pattern 3

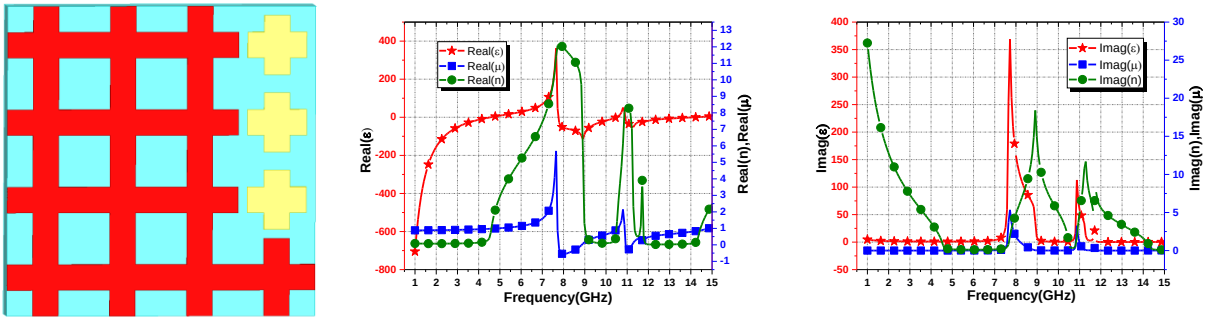

Figure II.28 Pattern3 with 3 disconnected cells(type B) and 13(type A) cells

- Pattern 4

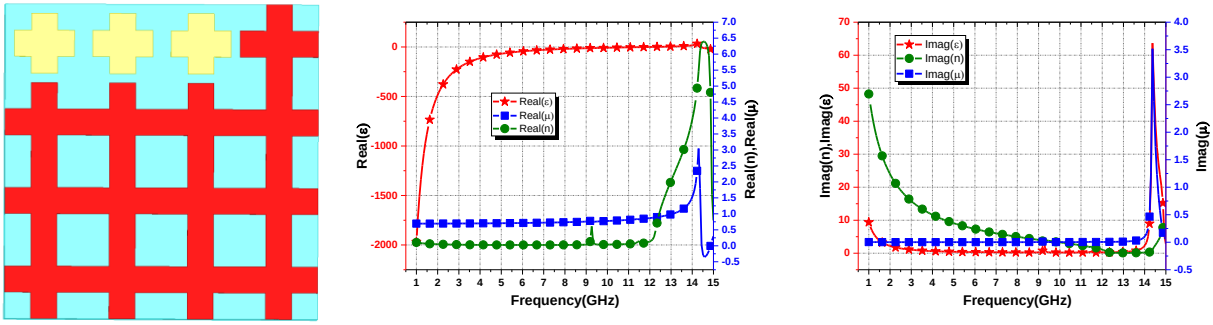

Figure II.29 Pattern4 with 3 disconnected cells(type B) and 13(type A) cells

II.4.4 Case IV (α=25%)

- Pattern 1

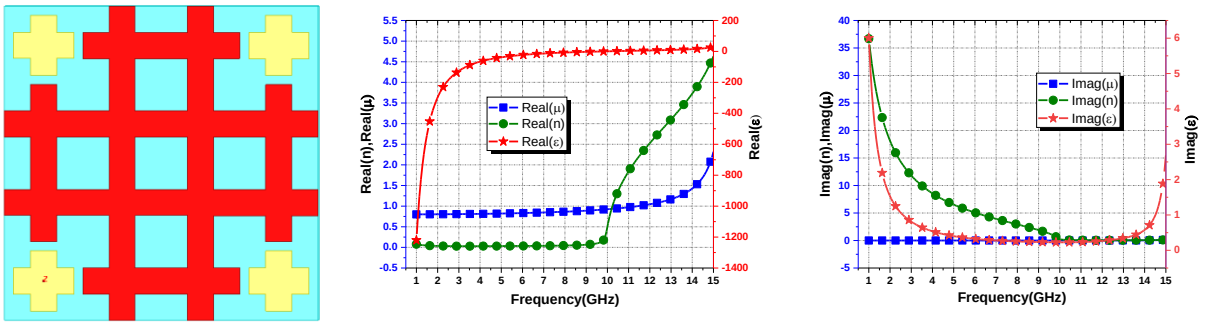

Figure II.30 Pattern1 with 4 disconnected cells(type B) and 12(type A) cells

- Pattern 2

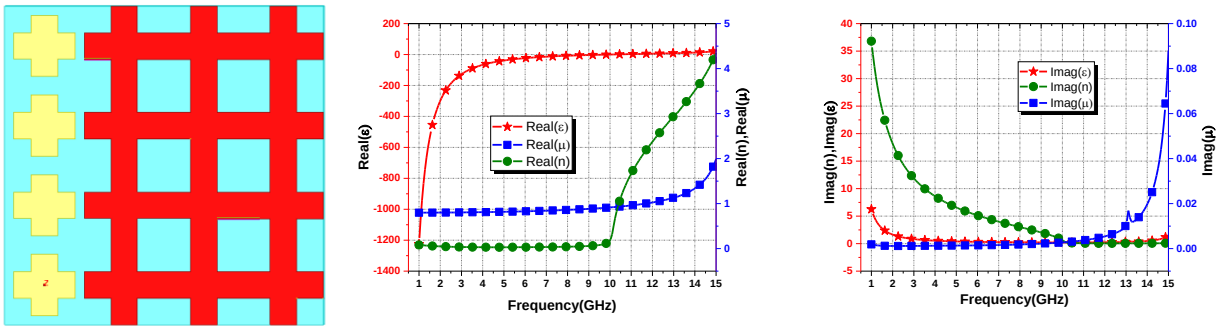

Figure II.31 Pattern2 with 4 disconnected cells(type B) and 12(type A) cells

- Pattern 3

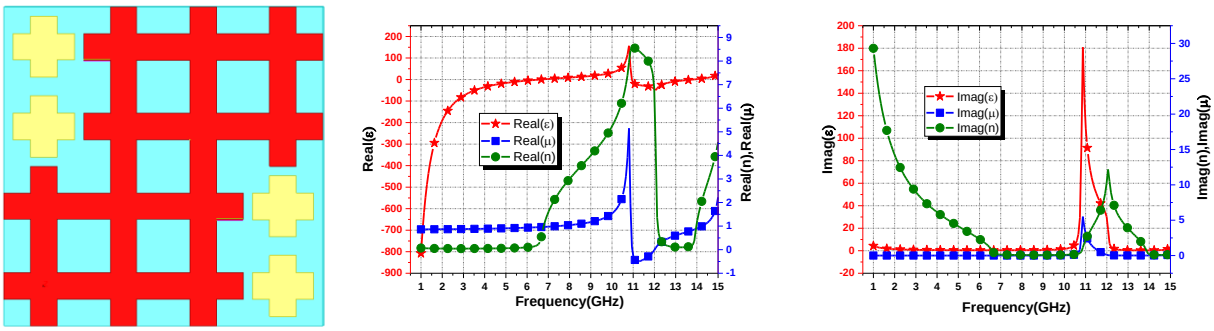

Figure II.32 Pattern3 with 4 disconnected cells(type B) and 12(type A) cells

- Pattern 4

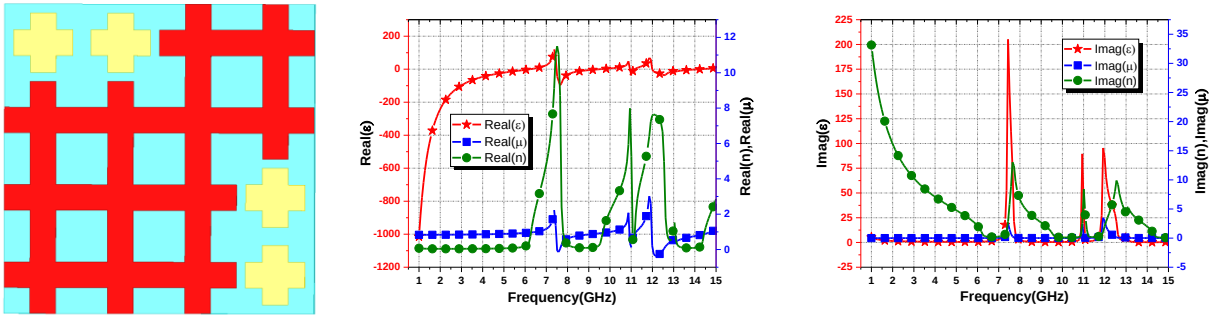

Figure II.33 Pattern4 with 4 disconnected cells(type B) and 12(type A) cells

II.5 Different results obtained

Table II.1 Results of Case II, Case III and Case IV

Pattern	Plasma frequency f_p	Refractive index n	Permittivity Ɛ	Permeability μ
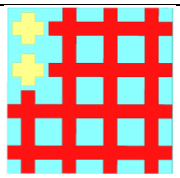	$f_p = 6.2$GHz	[0-6] n≈ 0 Peaks at 8GHz, 11GH,12GHz	$\varepsilon_{eff} < 11$	[0-6] $\mu_{eff} \approx 0$ Peaks at 7GHz, 10GH
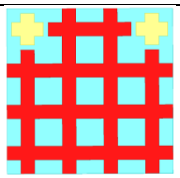	$f_p = 11.2$GHz	[0-11] n≈ 0 Peaks at 14GHz	$\varepsilon_{eff} < 43$	[0-11] $\mu_{eff} \approx 0$ Peaks at 14GHz
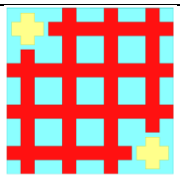	$f_p = 9.4$GHz	[0-9] n≈ 0 Peaks at 11GHz	$\varepsilon_{eff} < 90$	[0-9] $\mu_{eff} \approx 0$ Peaks at 11GHz

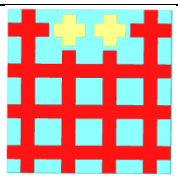	$f_p = 8.3\text{GHz}$	[0-7] n≈ 0 Peaks at 8.8GHz ,11.1GHz, 12.5GHz	$\varepsilon_{eff} < 65$	[0-7] $\mu_{eff} \approx 0$ Peaksat 8.8GHz ,11.1GHz, 12.5GHz
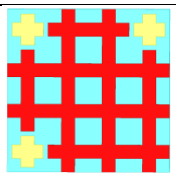	$f_p = 7.1\text{GHz}$	[0-6.5] n≈ 0 Peaks at 7GHz 10GHz,11GHz	$\varepsilon_{eff} < 43$	[0-6.5] $\mu_{eff} \approx 0$ Peaks at 14GHz
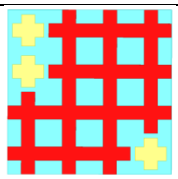	$f_p = 6.3\text{GHz}$	[0-6] n≈ 0 Peaks at 7GHz, 11GHz	$\varepsilon_{eff} < 100$	[0-6.5] $\mu_{eff} \approx 0$ Peaks at 7GHZ ,11GHz
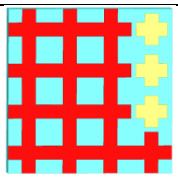	$f_p = 4.56\text{GHz}$	[0-4] n≈ 0 Peaks at 7.7GHz, 11GHz	$\varepsilon_{eff} < 360$	[0-4.7] $\mu_{eff} \approx 0$ Peaks at 7.6GHz
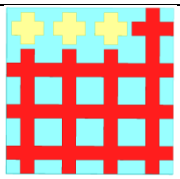	$f_p = 12.1\text{GHz}$	[0-11.7] n≈ 0 Peaks at 14.5GHz	$\varepsilon_{eff} < 46$	[0-11.7]$\mu_{eff} \approx 0$ Peaks at 14.3GHz
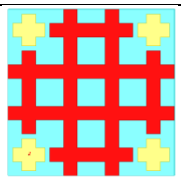	$f_p = 9.8\text{GHz}$	[0-9] n≈ 0 Peaks at 14GHz	$\varepsilon_{eff} < 22$	[0-10] $\mu_{eff} \approx 0$ Peaks at 14.8GHz

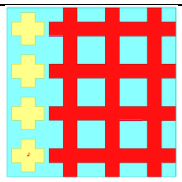	$f_p = 9.96$GHz	[0-9] n≈ 0 Peaks at 14.8GHz	$\varepsilon_{eff} < 20$	μ_{eff}<1.8
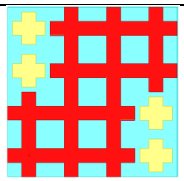	$f_p = 6.7$GHz	[0-6] n≈ 0 Peaks at 11.8GHz	$\varepsilon_{eff} < 156$	[0-7] $\mu_{eff} \approx 0$ Peaks at 10GHz
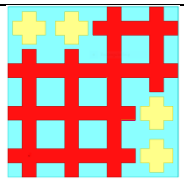	$f_p = 6.25$GHz	[0-6.1] n≈ 0 Peaks at 7GHz, 10GHz, 12GHz	$\varepsilon_{eff} < 120$	[0-6] $\mu_{eff} \approx 0$ Peaks at 7GHz, 11GHz

As we can see in the table above, we have different results with each pattern but overall we can say that the comportment of these supercells is always conductor.

II. 6 Conclusion

In this chapter we designed metamaterial supercells (4X4) based on connected unit cells(type A) and disconnected unit cells(type B), we also made a combination of both making different cases and different patterns and studying their results and their comportments.

We've noticed that the results change by changing the positions and number of connected unit cell (type A) and disconnected ones (type B), and the more there are cells type A the supercells comportment becomes more conductor and vise. And the more there are type B cells the supercells comportment becomes more dielectric.

In the next chapter we will design and make antennas based on the metamaterial supercells made in this chapter and see what results we get.

Chapter III

Metamaterial based Antennas

III- Metamaterial based Antennas

III.1 Introduction

In the previous chapter we have designed 4 cases of metamaterial supercells in the first case (Case I (α=6.25%)) we designed 10 different patterns, in the second one (Case II (α=12.5%)) we designed 4 different patterns, in the third one (Case III (α=18.75%)) we designed 4 different patterns as well as for (Case IV (α=25%)). In this chapter we will design a wifi patch antenna with f=2.4GHz based on those metamaterial super cells then we study its comportment compared to the classic copper wifi antennas.

III.2 Design of the patch antenna

A rectangular microstrip patch antenna is designed at resonant frequency of 2.4 GHz. The length (L) and width (W) and of the patch at a resonant frequency of 2.4 GHz is found to be 24 mm and 36 mm respectively, The height of the substrate is 1.6mm. The length (Lg) and width (Wg) of the ground plane is taken as 60mm and 60mm respectively. For feeding the microstrip patch antenna, inset feed technique is used having an inset length of 30 mm and width 3mm, and the gap width (Gf) is 0.5mm and length (Li) is 7mm . **Figure III.1** and **Figure III.2** show the frequency vs gain pattern of the antenna in the farfield. [19]

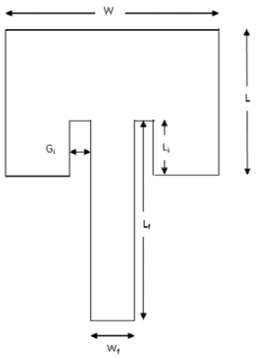

Figure III.1 Geometry of Inset fed Rectangular Patch Antenna

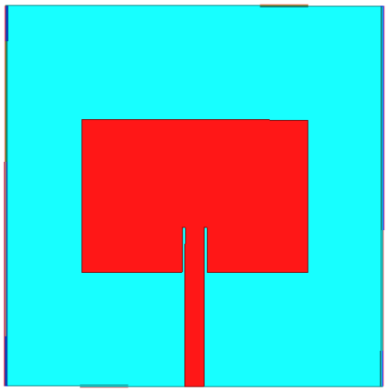

Figure III.2 Antenna Geometry

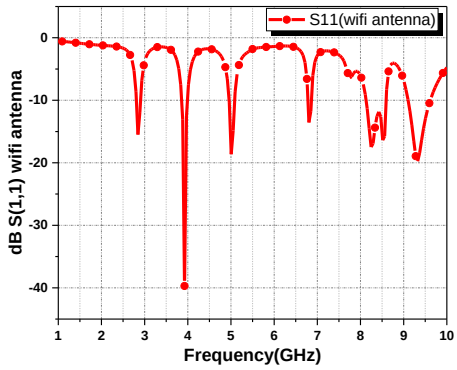

Figure III.3 dB(S(1,1)) of a copper wifi antenna

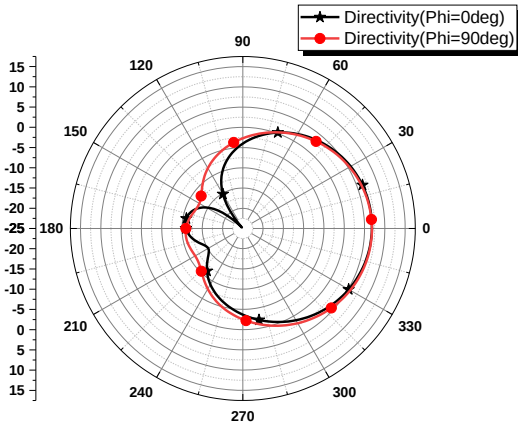

Figure III.4 Radiation pattern in E (Phi=0°)and H (Phi=90°)

Figure III.3 and **Figure III.4** represent the results of the simulations of the antenna shown in **Figure III.2**. As we can see there are 7 resonant frequencies: f1=2.8GHz, f2=3.9GHz, f3=4.9GHz, f4=6.8GHz, f5=8.2GHz, f6=8.5GHz, f7=9.3GHz and their corresponding adaptation: -15.4dB, -39.8dB, -18.4dB, -13.2dB, -17.7dB, -16.1dB, -19.6dB respectively. And a directivity of 6.95dB both at 0° and 90°.

III.3 Metamaterial Supercells based Antennas

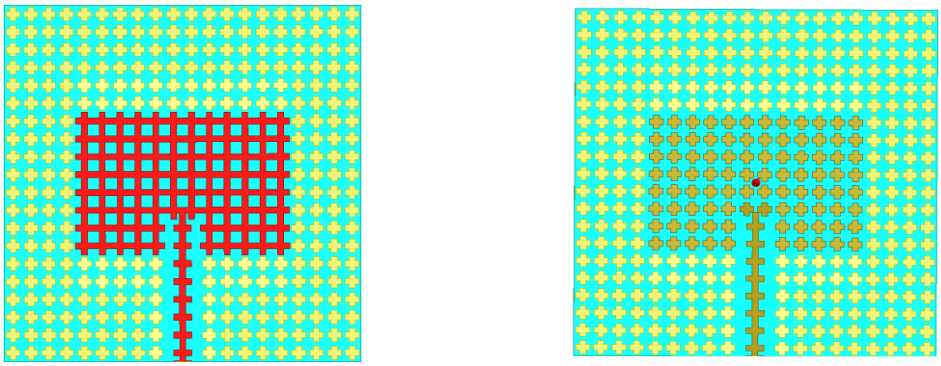

Type A suppercell Ant Type B suppercell Ant

Figure III.5 Metamaterial Antennas

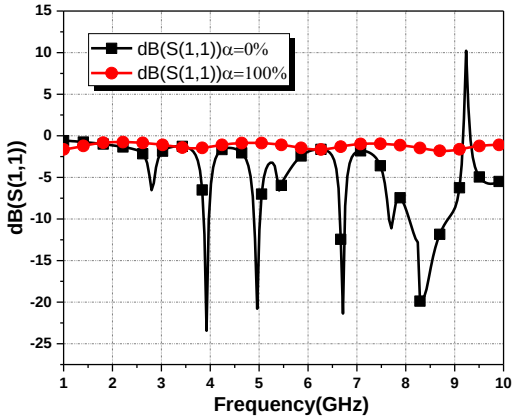

Figure III.6 dB(S(1,1)) of all connected cells antenna(α=0%) and all disconnected cells antenna(α=100%)

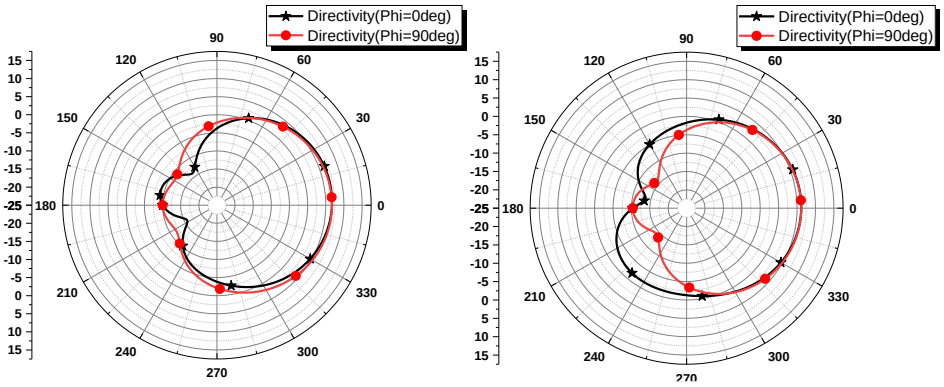

Radiation pattern Ant (A) Radiation pattern Ant (B)

Figure III.7 Radiation pattern in E (Phi=0°)and H (Phi=90°)

When designing metamaterial based antennas we started with pattern A and B as shown in **Figure III.5**. We notice in the results shown in **Figure III.6**, that type A antenna (α=0%) is well adapted and has 4 resonant frequencies: f1=3.9GHz, f2=4.9GHz, f3=6.7GHz, f4=8.3 with the corresponding adaptation respectively: -23.3dB, -20.7dB, -21.3, -20; and a directivity of 6.7dB both at 0°and 90° **Figure III.7**. It also shows that type B antenna (α=100%) is poorly adapted and has a directivity of 5.9dB.

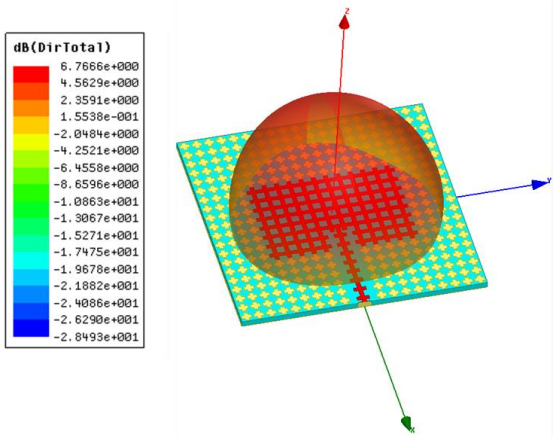

Figure III.8 Radiation pattern of a type A supercell antenna

III.4 Cases and patterns

III.4.1 Case I (α=6.25%)

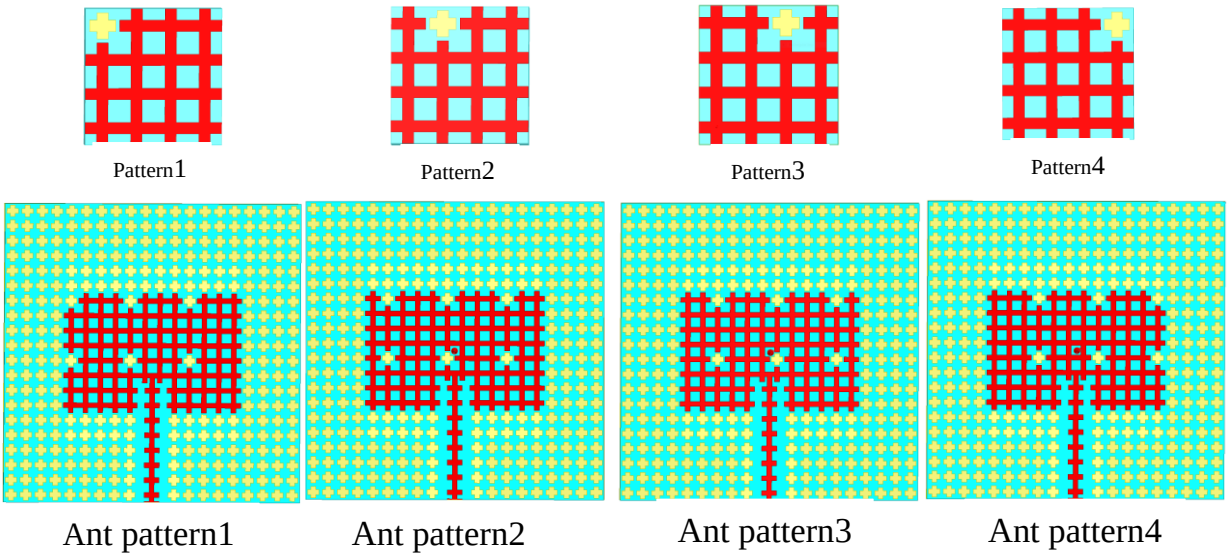

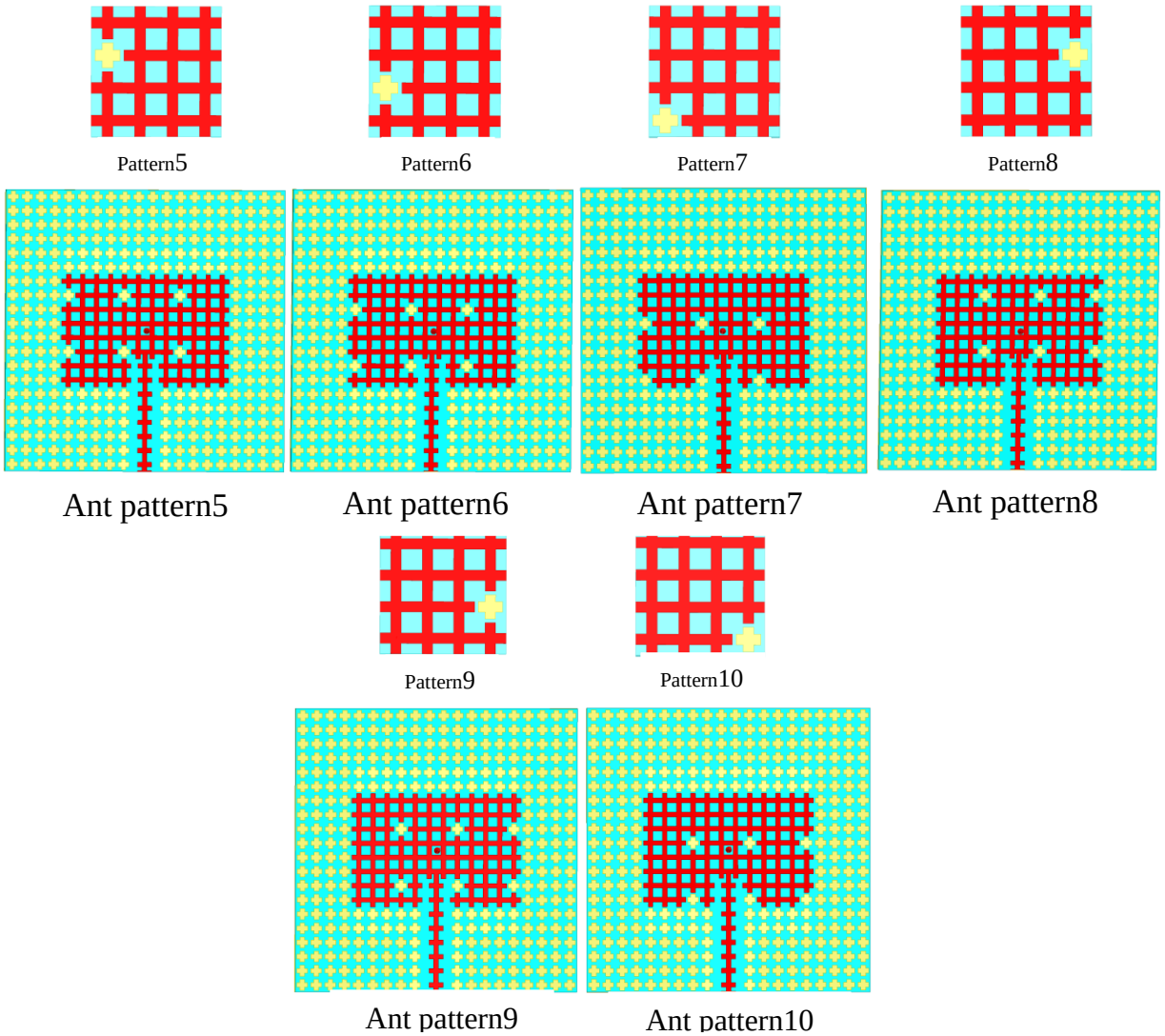

Figure III.9 Metamaterial Antennas of Case I(α=6.25%)

In this case we change the position of the disconnected cell horizontally then vertically to see the effect it has on the antenna and we got the following results (**Figure III.9**, **Figure III.10**, **Table III.1**).

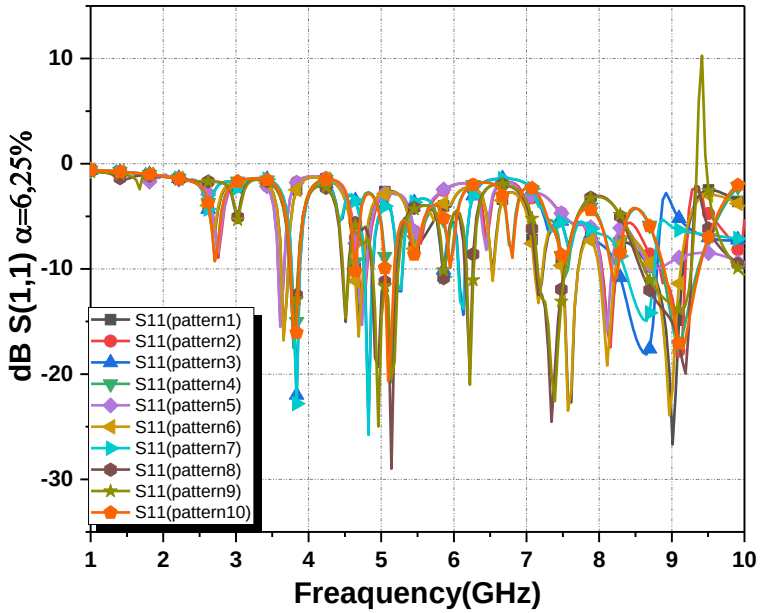

Figure III.10 dB(S(1,1)) of all 10 Patterns of Case I (α=6.25%)

Due to similarities of the results of the Patterns in Case I, for a clearer view of the results we chose 3 Patterns with different results (**Figure III.11**).

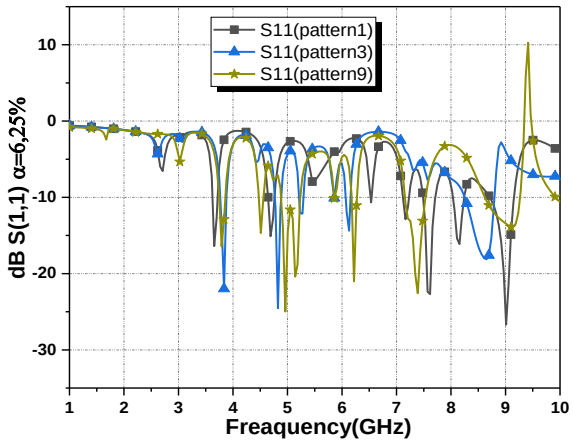

Figure III.11 dB(S(1,1)) of 3 different patterns of Case I

Table III.1 Metamaterial Antenna parameters of Case I (α =6.25%)

α =6.25%	Directivity(dB)	S(1,1)(dB)	Frequency(GHz)
Pattern 1	6.7	-16.4	3.6
		-14.9	4.6
		-12.6	7.1
		-22.5	7.6
		-16.01	8.1
		-26.3	9.02
Pattern3	6.7	-21.6	3.8
		-24.5	4.8
		-12	5.2
		-14.3	6.1
		-18.1	8.6
Pattern9	6.7	-16.4	3.8
		-14.5	4.5
		-24.9	4.9
		-19.9	5.1
		-20.9	6.2
		-22.7	7.3
		-13.9	9

The parameters in **Table III.1** and the results in **Figure III.11** show the well adaptation these antennas and that we can obtain a new antenna with different parameters by merely changing the position of the disconnected cell.

III.4.2 Case II (α=12.5%)

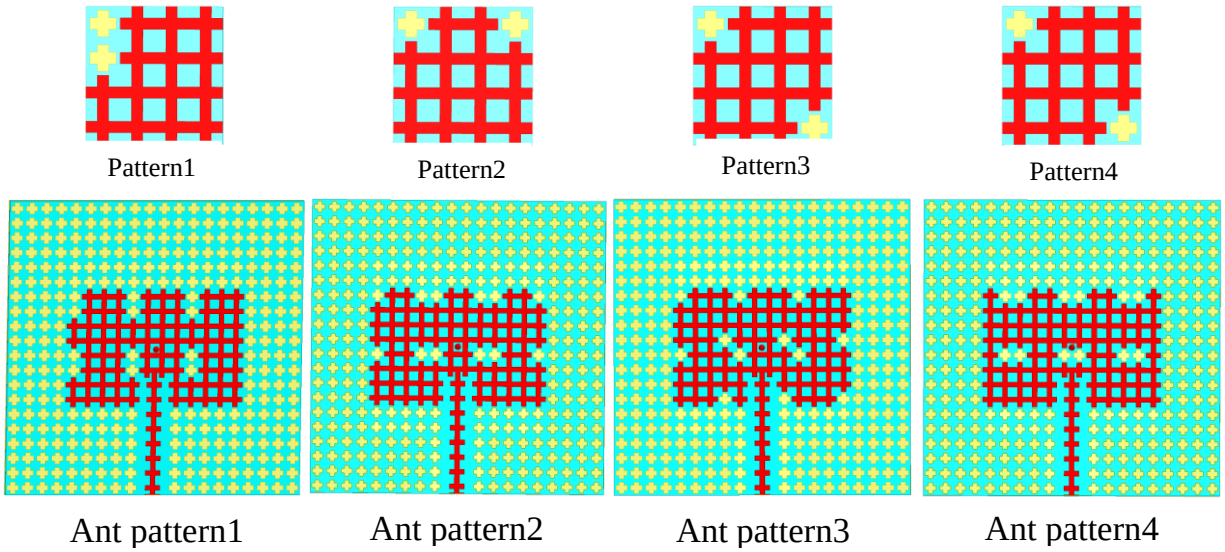

Figure III.12 Metamaterial Antennas of Case II (α=12.5%)

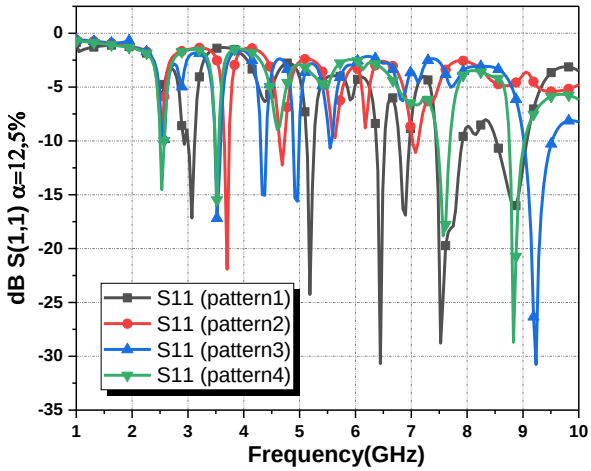

Figure III.13 dB(S(1,1) of all 10 Patterns of Case II(α=12.5%)

Table III.2 Metamaterial Antenna parameters of Case II (α =12.5%)

α=12.5%	Directivity(dB)	S11(dB)	Frequency(Ghz)
Pattern 1	6.3	-17	3.07
		-24.1	5.2
		-30.6	6.4
		-16.6	6.8
		-28.5	7.5

		-15.9	8.8
Pattern 2	6.9	-9.6	2.5
		-21.9	3.7
		-12.01	4.6
		-11	7.08
Pattern 2	6.7	-17.1	3.5
		-14.9	4.3
		-15.4	4.9
		-30.6	9.23
Pattern 4	6.3	-14.5	2.5
		-15.4	3.5
		-18.2	7.5
		-28.7	8.8

Table III.2 and **Figure III.13** show that we have a whole new results and parameters by changing the percentage of the disconnected cell. The comportment is still conductor but we see a lot of changes in the adaptability.

III.4.3 Case III (α=18.75%)

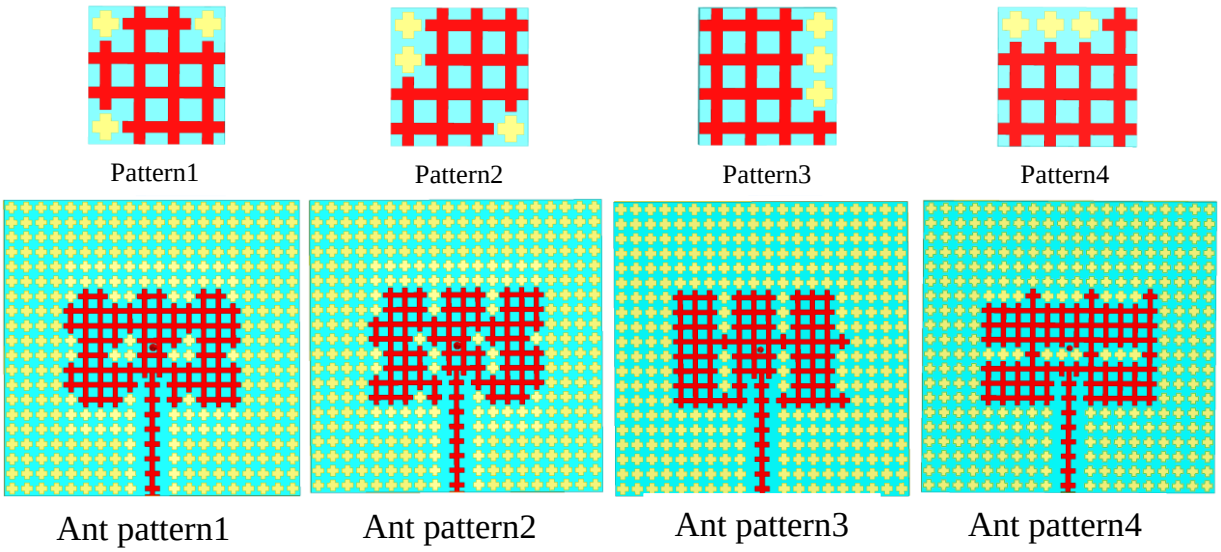

Figure III.14 Metamaterial Antennas of Case III (α=18.75%)

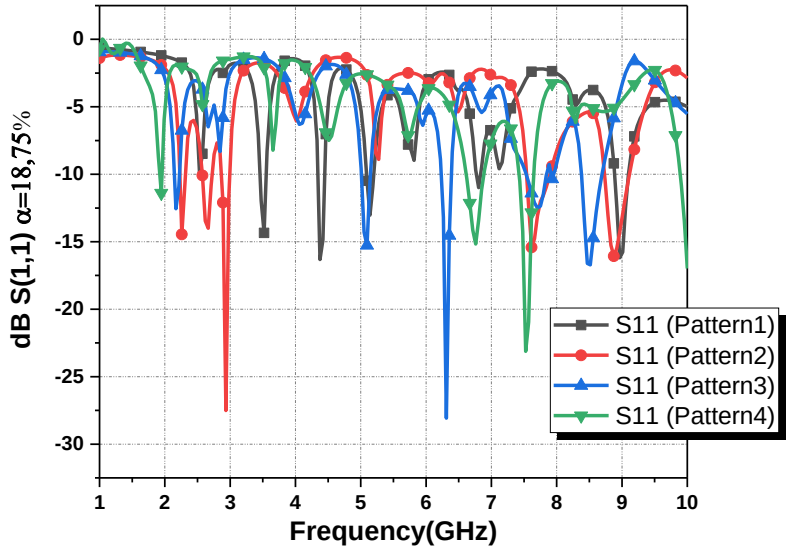

Figure III.15 dB(S(1,1) of all 4 patterns of Case III (α=18.75%)

Table III.3 Metamaterial Antenna parameters of Case III (α=18.75%)

α=18.75%	Directivity(dB)	S(1,1)(dB)	Frequency(GHz)
Pattern1	6.5	-14.5	3.5
		-16.2	4.3
		-12.9	5.1
		-15.8	8.9
Pattern2	6.5	-14.4	2.2
		-13.8	2.6
		-27.3	2.9
		-15.5	7.5
		-16	8.8
Pattern3	6.5	-12.4	2.1
		-15	5
		-27.9	6.3
		-12.3	7.7
		-16.6	8.5
Pattern4	5.4	-11.4	1.9
		-15	6.7
		-23	7.5

In Figure III.15 and Table III.3 we notice a poor adaptability of the antenna in Pattern3 and Pattern4 compared to Pattern1 and Pattern2 because as we can see in the design of the corresponding supercells an antennas the alignment of the disconnected cells make an obstacle for the feeding to go through to the rest of the cells.

III.4.4 Case IV (α=25%)

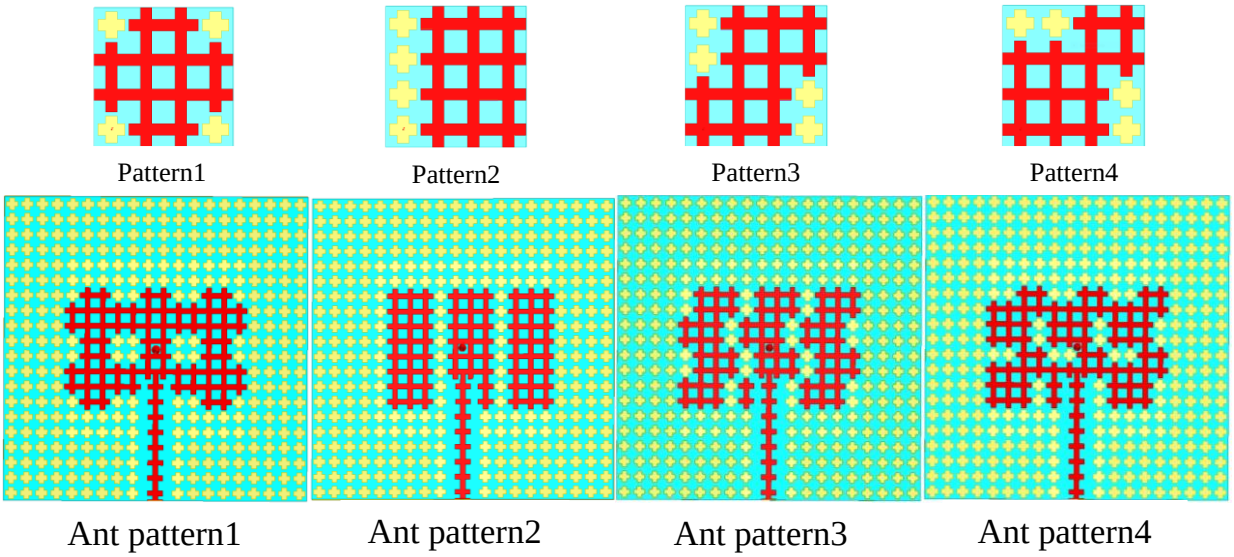

Figure III.16 Metamaterial Antennas of Case IV (α=25%)

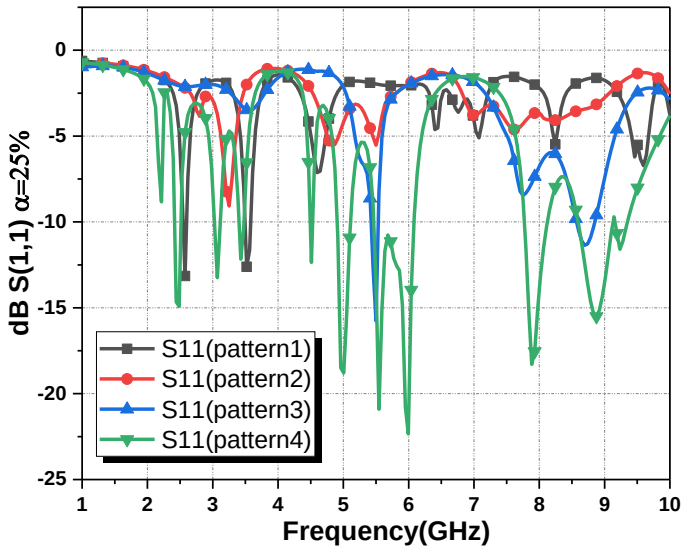

Figure III.17 dB(S(1,1) of all 4 patterns of Case IV (α=25%)

Table III.4 Metamaterial Antenna parameters of Case IV (α=25%)

α=25%	Directivity(dB)	S(1,1)(dB)	Frequency(GHz)
Pattern1	6.7	-13.1	2.5
		-12.7	3.5
Pattern2	6.7	/	/
Pattern3	6.5	-15.6	5.5
		-11.3	8.6
Pattern 4	5.9	-14.7	2.4
		-13.1	3
		-11.9	3.4
		-12.2	4.5
		-18.7	4.9
		-20.8	5.5
		-22.3	6
		-17.9	7.9
		-15.4	8.8

Same as in case III we notice that in Pattern2 there's a poor adaptability due to the blockage of the feeding.

III.5 Fabricated Antenna based on metamaterial supercells

The fabricated prototype (**Figure III.18)** presents as a wifi patch antenna based on metamaterial supercells with dimensions of 60 mm×60 mm fabricated on a FR-4 Substrate. The chosen substrate exhibits a relative dielectric constant of ε_r= 4.4, and a thickness of h=1.6mm and operates at a frequency of 2.4GHz. The conductive elements of the antenna and the metamaterial structure are realized using copper.

The copper metallic patterns (metamaterial supercell type A pattern) are clearly visible on the brown/green substrate. A prominent feature is the distinct arrangement of the metamaterial supercells: a central square region populated by a grid of etched square patterns (connected cells which play the role of a perfect conductor), surrounded by an outer perimeter of intricately etched plus-shaped (+) patterns (disconnected cells which play the role of a dielectric). An SMA connector is mounted on the left edge, facilitating signal input/output via a microstrip feed line. The robust construction and visible precision in the etched patterns reflect the meticulous fabrication process. Its compact and visually distinct design makes it suitable for integration into various modern wireless systems.

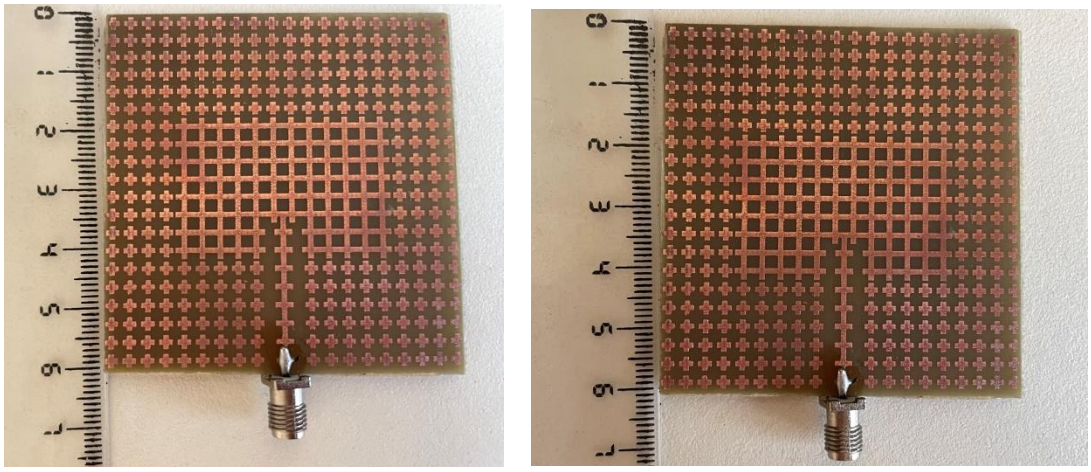

Figure III.18 A prototype of a metamaterial supercell based patch antenna

We connected the antenna to an Anritsu VectorStar Vector Network Analyzer (VNA) (**Figure III.19)** after calibrating it and entering the frequency band (1GHz-10GHz) . We got the results shown in **Figure III.20**.

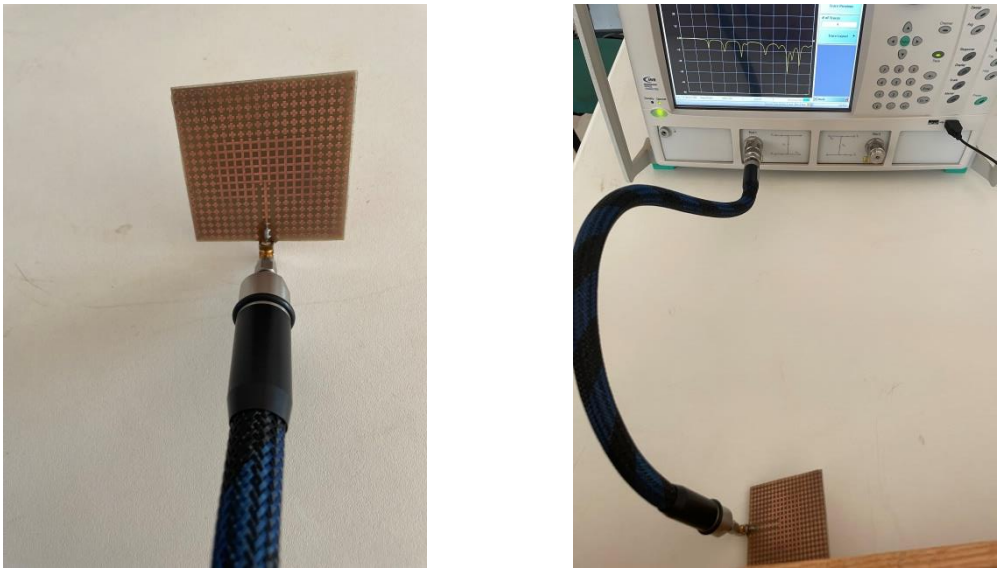

Figure III.19 The prototype patch antenna connected to VNA

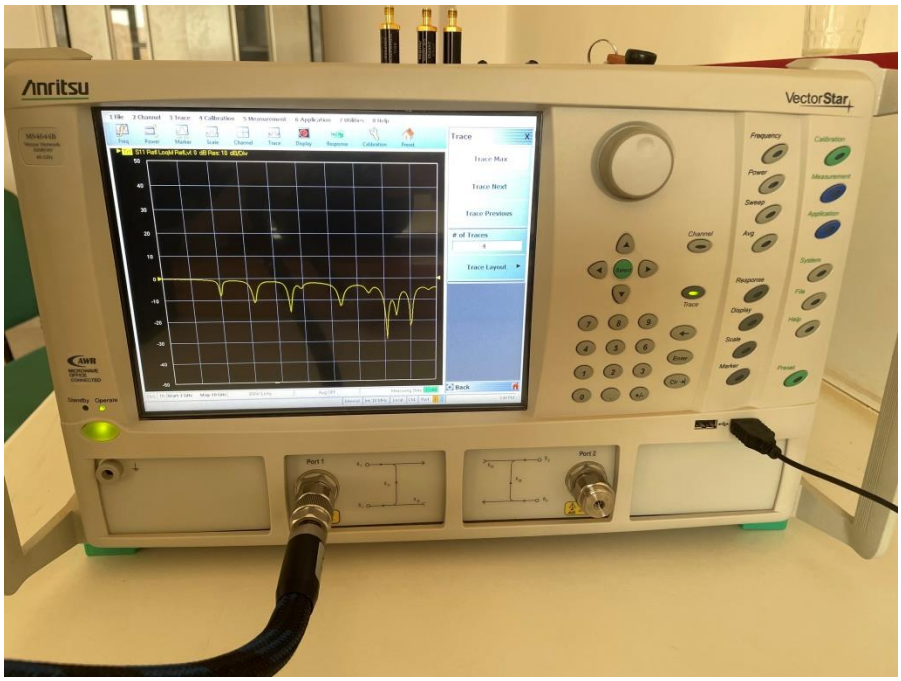

Figure III.20 The results Obtained on the Analyser(VNA)

And after exporting them and comparing them to the simulation we got the following result (**Figure III.21**) :

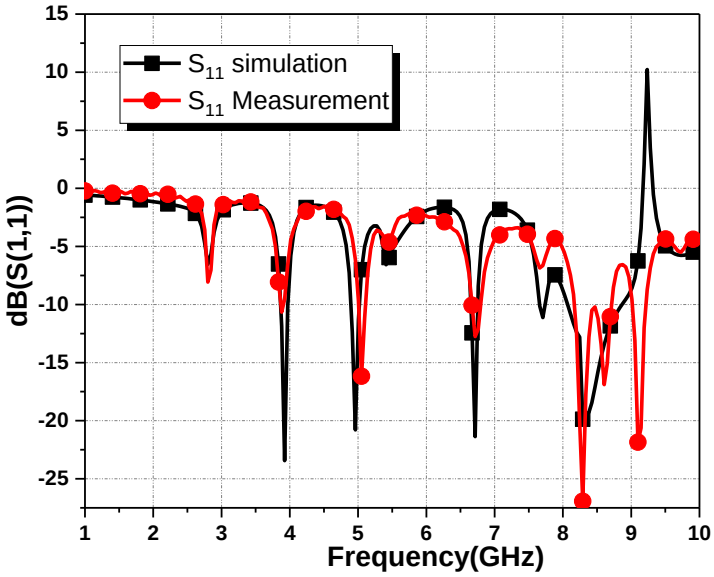

Figure III.21dB(S(1,1) of the metamaterial supercell antenna (simulation and mesurement)

As shown in **Figure III.21** we got a very good result where the simulation adaptation is fairely close to the mesurement adaptation. The deformation is most probably due to the hardship we found with the antenna connected. We had to change it twice due to its malfunction, and that resulted in lusing a part of a few cells on the feed line.

The results are still considered pretty close and fairely good .

III.6 Conclusion

This chapter successfully presented the comprehensive design and analysis of a Wi-Fi patch antenna operating at 2.4 GHz, fundamentally enhanced by the integration of metamaterial supercells. Building upon the foundational metamaterial unit cell designs established in the preceding chapter, we systematically explored four distinct cases of supercell configurations (Case I (α=6.25%), Case II (α=12.5%), Case III (α=18.75%), and Case IV (α=25%), each comprising various patterns.

The primary objective of this chapter was to leverage these meticulously designed metamaterial structures to optimize the performance of a standard Wi-Fi patch antenna.

Through rigorous simulation and, presumably, experimental validation (as discussed in the chapter's body), the comportment of the metamaterial-integrated antenna was thoroughly investigated. A critical aspect of this study involved a direct comparative analysis between the developed metamaterial-based antenna and its classic copper Wi-Fi antenna counterpart.

General Conclusion

The ever-increasing demand for advanced wireless communication systems necessitates highly adaptive and efficient antenna solutions capable of dynamic control over their operating parameters. This thesis successfully addressed this critical need by proposing, designing, simulating, and fabricating a novel reconfigurable metamaterial supercell aimed at dynamically controlling the operating frequency of printed antennas.

The foundational principle of this work relied on leveraging the unique electromagnetic properties of metamaterials, specifically by designing unit cells with distinct refractive indices—the connected cross-type (A) with a near-zero index and the disconnected cross-type (B) with an index slightly greater than unity. A significant contribution of this research lies in the development of a switching mechanism that allows for the arbitrary spatial distribution of these unit cell types within a 4x4 supercell. This innovation enables real-time reconfiguration of the supercell's overall electromagnetic response, a capability crucial for adaptive antenna systems.

Comprehensive electromagnetic simulations, guided by the homogenization criterion and subwavelength operation at 2.4 GHz, meticulously characterized the behavior of various supercell configurations. These simulations demonstrated the profound influence of the proportion and spatial arrangement of disconnected unit cells on the effective parameters of the supercell. Importantly, the research successfully linked these reconfigurable metamaterial properties to the control of an integrated patch antenna's resonant frequency. By systematically varying the percentage of disconnected cross-type B elements (6.25%, 12.5%, 18.75%, and 25%), and their arbitrary positioning, a robust method for frequency tuning was established. This dynamic tunability, achieved through the manipulation of switching states, represents a significant step towards realizing truly smart antenna systems.

General Conclusion

In conclusion, this thesis presents a viable and effective approach for enhancing the adaptability of printed antennas through the integration of reconfigurable metamaterial supercells. The methodology, encompassing detailed design, rigorous simulation, and the successful demonstration of frequency control via a programmable metamaterial structure, offers a promising pathway for future developments in reconfigurable RF devices. The insights gained from the characterization of these metamaterial supercells and their impact on antenna performance lay a strong foundation for further research into advanced beamforming, multi-band operation, and adaptive stealth technologies.

References

[1] Hasar, Ugur Cem, et al. "Determination of effective constitutive parameters of inhomogeneous metamaterials with bianisotropy." *IEEE Transactions on Microwave Theory and Techniques* 66.8 (2018): 3734-3744.

[2] https://www.slideshare.net/slideshow/smart-materials-30408850/30408850

[3] Qader, Ibrahim Nazem, et al. "A review of smart materials: researches and applications." *El-Cezeri* 6.3 (2019): 755-788.

[4] Spaggiari, Andrea, et al. "Smart materials: Properties, design and mechatronic applications." *Proceedings of the institution of mechanical engineers, part l: journal of materials: design and applications* 233.4 (2019): 734-762.

[5] https://builtin.com/articles/smart-materials

[6] https://en.wikipedia.org/wiki/Smart_material

[7] https://www.britannica.com/topic/metamaterial

[8] https://en.wikipedia.org/wiki/Metamaterial

[9] Youn, S. J., et al. "Extended Drude model analysis of noble metals." *physica status solidi (b)* 244.4 (2007): 1354-1362.

[10] Wang, Heng, et al. "Extended Drude model for intraband-transition-induced optical nonlinearity." *Physical Review Applied* 11.6 (2019): 064062.

[11] https://empossible.net/wp-content/uploads/2018/03/Lecture-2-Lorentz-and-Drude-models.pdf

[12]https://physics.byu.edu/faculty/colton/docs/phy442-winter20/lecture-11-lorentz-oscillator-model.pdf

[13] Oughstun, Kurt E., and Natalie A. Cartwright. "On the Lorentz-Lorenz formula and the Lorentz model of dielectric dispersion." *Optics express* 11.13 (2003): 1541-1546.

[14]https://www.everythingrf.com/community/what-are-metamaterials-and-what-are-they-used-for_1588

[15] https://en.wikipedia.org/wiki/Negative-index_metamaterial

References

[16] Smith, D. Robert, et al. "Determination of effective permittivity and permeability of metamaterials from reflection and transmission coefficients." *Physical review B* 65.19 (2002): 195104.

[17] https://optics.org/news/12/7/1

[18] https://article.murata.com/en-global/article/what-is-a-metamaterial

[19] https://ijrpr.com/uploads/V4ISSUE6/IJRPR14277.pdf

[20]Bouras, Khedidja, et al. "Frequency Agile Bilayer Metamaterials for Radar Cross-Section Reduction." *Journal of Electronic Materials* 53.11 (2024): 7132-7139